AD-752 900

RADAR CROSS-SECTION MEASUREMENTS OF SNOW AND ICE

Pieter Hoekstra, et al

Cold Regions Research and Engineering Laboratory

Prepared for:

Advanced Research Projects Agency

November 1972

TR 235

Technical Report 235

RADAR CROSS-SECTION MEASUREMENTS OF SNOW AND ICE

Pieter Hoekstra and Dennis Spanogle

November 1972

CORPS OF ENGINEERS, U.S. ARMY
COLD REGIONS RESEARCH AND ENGINEERING LABORATORY
HANOVER, NEW HAMPSHIRE

Unclassified

Security Classification

DOCUMENT CONTROL DATA - R & D

(Security classification of title, body of abstract and indexing annotation must be entered when the overall report is classified)

1. ORIGINATING ACTIVITY *(Corporate author)*
U.S. Army Cold Regions Research and Engineering Laboratory
Hanover, New Hampshire

2a. REPORT SECURITY CLASSIFICATION
Unclassified

2b. GROUP

3. REPORT TITLE

RADAR CROSS-SECTION MEASUREMENTS OF SNOW AND ICE

4. DESCRIPTIVE NOTES *(Type of report and inclusive dates)*

5. AUTHOR(S) *(First name, middle initial, last name)*

Pieter Hoekstra and Dennis Spanogle

6. REPORT DATE	7a. TOTAL NO. OF PAGES	7b. NO. OF REFS
November 1972	43	9

8a. CONTRACT OR GRANT NO.	9a. ORIGINATOR'S REPORT NUMBER(S)
ARPA Order 1615	
b. PROJECT NO.	Technical Report 235
c.	9b. OTHER REPORT NO(S) *(Any other numbers that may be assigned this report)*
d.	

10. DISTRIBUTION STATEMENT

Approved for public release; distribution unlimited.

11. SUPPLEMENTARY NOTES	12. SPONSORING MILITARY ACTIVITY
	Advanced Research Projects Agency

13. ABSTRACT

The radar backscatter from undisturbed snow surfaces was measured at 10 GHz, 35 GHz and 95 GHz and at grazing angles of 1 to 0.4°. For horizontally polarized radiation the ground clutter per unit area (m^2) at 10 GHz from a flat snow terrain decreased from -50 db at 1° to -70 db at 0.4°. The return was approximately 10 db lower for vertically polarized radiation. The ground clutter depended on the free water content of the snow. The return at 35 GHz was approximately 10 db higher than that at 10 GHz at horizontal and vertical polarizations and at a grazing angle of 0.4°. The difference between the return at 10 GHz and that at 35 GHz decreased at higher grazing angles. Because of its narrow beamwidth the 95-GHz radar saw individual patches in the terrain and no meaningful number for the terrain radar cross section could be obtained. The radar cross section of ice blocks placed on the snow surface was roughly proportional to the square of the area of the ice blocks facing the radar at 10 and 35 GHz and was about 20 dbsm below the return expected for a perfectly reflecting plane surface. At 95 GHz the ice blocks became diffuse reflectors. The power reflection coefficient at normal incidence for ice blocks with carefully prepared surfaces measured in free space was from 0.005 to 0.08 at 10 GHz and from 0.009 to 0.031 at 35 GHz.

14. Key Words

Dielectric properties
Ground clutter
Radar cross sections
Snow and ice surfaces
Terrain avoidance

DD FORM 1 NOV 68 1473 REPLACES DD FORM 1473, 1 JAN 64, WHICH IS OBSOLETE FOR ARMY USE.

Unclassified

Security Classification

RADAR CROSS-SECTION MEASUREMENTS OF SNOW AND ICE

Pieter Hoekstra and Dennis Spanogle

November 1972

PREPARED FOR
ADVANCED RESEARCH PROJECTS AGENCY
ARPA ORDER 1615
BY
CORPS OF ENGINEERS, U.S. ARMY
COLD REGIONS RESEARCH AND ENGINEERING LABORATORY
HANOVER, NEW HAMPSHIRE

PREFACE

This report was prepared by Dr. Pieter Hoekstra, Research Physicist, of the U.S. Army Cold Regions Research and Engineering Laboratory (USA CRREL), and Mr. Dennis Spanogle of General Dynamics, Convair Aerospace Division, Fort Worth, Texas. The program was under the direction of Dr. Pieter Hoekstra and was supported by Advanced Research Projects Agency Order 1615.

Thanks are due the following for their help and interest in this experimental program: Mr. F.C. Paddison of the Applied Physics Laboratory, Johns Hopkins University; Messrs. R.B. Landers and M. Moore of the Radar Target Scattering (RATSCAT) facility, 6585th Test Group, Holloman Air Force Base; Mr. M. Foral of the Naval Air Development Center; and Messrs. B. Chapman, A. Delaney, and R. May, Drs. C. Keeler and R. Manis, and SP5 P. Cappillino of USA CRREL.

The *X*-band and *K*a-band systems were transported from New Mexico and Texas to New Hampshire and returned to their points of origin after completion of the tests by the New Hampshire Air National Guard stationed at Pease Air Force Base, Portsmouth, New Hampshire.

CONTENTS

ILLUSTRATIONS

CONTENTS (Cont'd)

ILLUSTRATIONS (Cont'd)

TABLES

CONTENTS (Cont'd)

TABLES (Cont'd)

RADAR CROSS-SECTION MEASUREMENTS OF SNOW AND ICE

by

Pieter Hoekstra and Dennis Spanogle

INTRODUCTION

As part of an Advanced Research Projects Agency (ARPA) program to develop a surface effect vehicle (SEV) for use in the Arctic, measurements of the backscatter from snow and ice surfaces were obtained for the design of a terrain avoidance system. This report presents the results of these measurements and describes the procedures used to obtain them.

In terrain avoidance systems a laser usually gives high resolution, but fails in detecting objects during falling and blowing snow and ice and water fog. During such conditions a radar system is needed for the reliable detection of objects, because radar can penetrate snow and fog.

Since the SEV moves close to the surface and elaborate antenna towers therefore are not feasible, the radar system must scan the surface at low grazing angles, 1° and lower. For the design of this radar, the following environmental parameters are required to optimize the system:

1. the terrain clutter from snow and ice surfaces at low grazing angles and at various frequencies
2. the radar cross section of ice and snow obstacles.

A test plan to measure these radar parameters was made with the close cooperation of the Applied Physics Laboratory, Johns Hopkins University; the Radar Target Scattering (RATSCAT) facility, 6585th Test Group, Holloman Air Force Base; and the U.S. Army Cold Regions Research and Engineering Laboratory (USA CRREL). The Applied Physics Laboratory, Johns Hopkins University was charged with the preliminary design of a pilotage system for the SEV.

The 10-GHz (*X*-band) radar equipment was supplied by the RATSCAT facility. The operation and maintenance of this facility at the time of the tests were contracted to General Dynamics, Convair Aerospace Division, Fort Worth, Texas.

The 35-GHz (*K*-band or *Ka*-band) radar system (transmitter, receiver, mixer and antenna structure) was loaned on a no-cost basis by General Dynamics, Convair Aerospace Division, Fort Worth, Texas. This radar was interfaced with the RATSCAT intermediate frequency amplifier and video processing system to obtain data compatible with the *X*-band data. Both the *X*-band and *Ka*-band systems were operated by RATSCAT personnel.

The 95-GHz (*V*-band) radar system was supplied by the Naval Air Development Center, Johnsville, Pennsylvania, and was operated by Navy personnel.

The measurements were made on a snow and ice covered lake in Lyme, New Hampshire. The radars were placed on the shore at the edge of the lake. The distance to the shore on the other

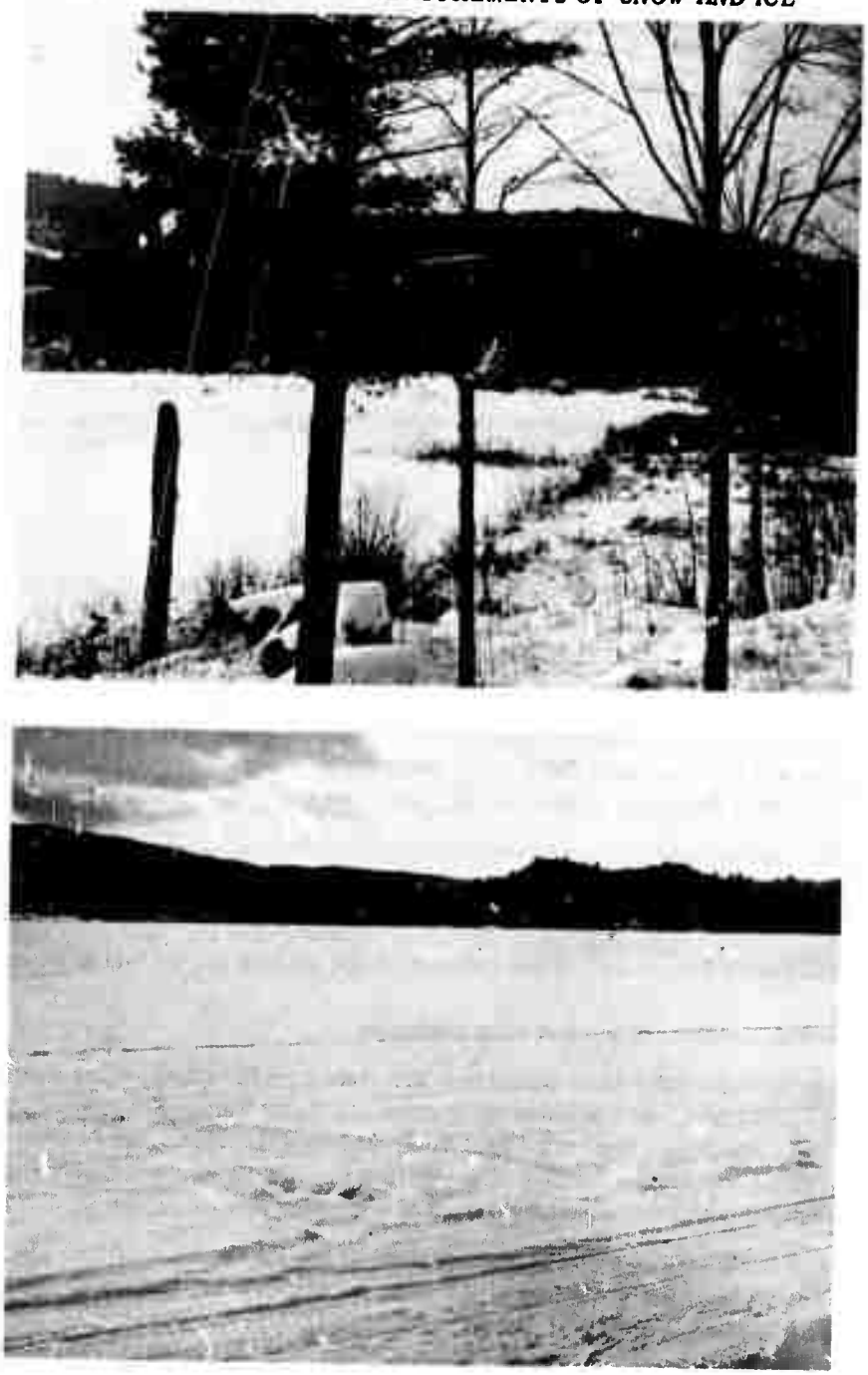

Figure 1. Post Pond site at Lyme, New Hampshire.

side of the lake was 2000 ft. The tests were conducted from 10 January 1971 to 15 March 1971. Views of the site are given in Figure 1. A schematic layout of the site is given in Figure 2. The placement of the radar systems is shown in Figure 3.

During this program the depth of the snow overlying the fresh-water ice varied from 0 to 12 in. and the state of the snow varied from dry, loose powder to wet slush. The state of the snow cover was recorded daily during the radar experiments. Measurements were made of snow depth, snow temperature and snow density.

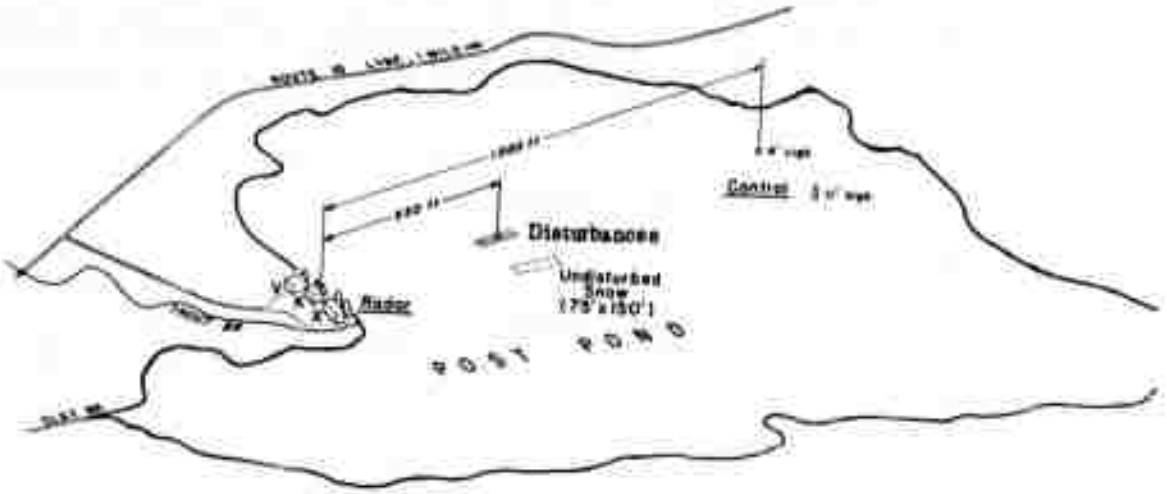

Figure 2. Schematic layout of the radar site.

Figure 3. Placement of the three radars.

In some measure the data of backscatter from the snow and ice surfaces are influenced by the dielectric behavior of snow and ice and by the variation of these properties in a natural environment. Therefore, a review of the literature on the dielectric behavior of snow and ice surfaces is included in this report.

REVIEW OF LITERATURE

Dielectric behavior of water and ice

For both water and ice, the relative dielectric constant ϵ'/ϵ_0 and the dielectric loss ϵ''/ϵ_0 traverse in first approximation a simple Debye relaxation spectrum (Eisenberg and Kauzmann 1969)

$$\frac{\epsilon' - \epsilon'_\infty}{\epsilon_0} = \frac{(\epsilon'_s - \epsilon'_\infty)}{\epsilon_0(1 + \omega^2\tau^2)}$$

$$\frac{\epsilon''}{\epsilon_0} = \frac{(\epsilon'_s - \epsilon'_\infty)\omega\tau}{\epsilon_0(1 + \omega^2\tau^2)}$$

where ω is the angular frequency; subscripts s and ∞ refer to the static and high-frequency dielectric constants respectively; τ is the relaxation time; and ϵ_0 is the permittivity of free space, 8.85×10^{-12} farad/m.

The chief difference between the dielectric behavior of pure ice and that of pure water is that the relaxation time of water is 6 powers of 10 smaller than that of ice. This difference is shown in Figure 4, which gives the dielectric relaxation spectra of water and ice.

The dielectric loss of water at low frequency is caused by ions, protons and hydroxyls. The dielectric loss caused by a d-c conductivity decreases with frequency according to the relation

$$\frac{\epsilon''(\omega)}{\epsilon_0} = \frac{\sigma}{\epsilon_0\omega}$$

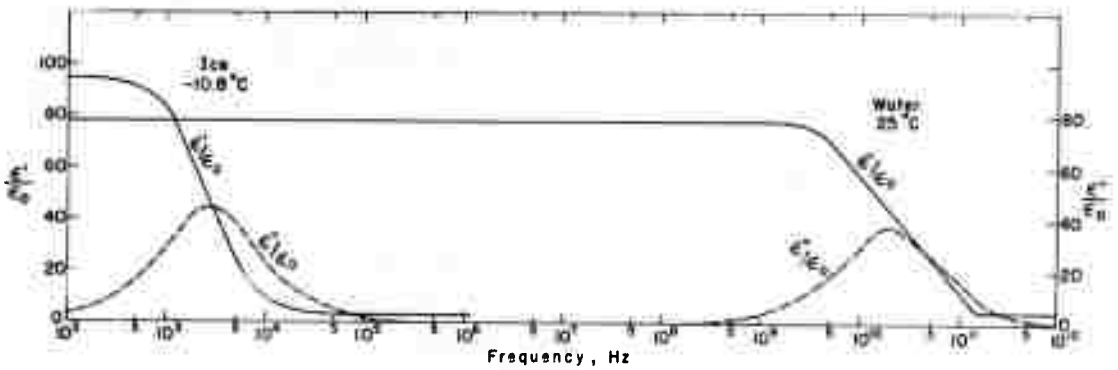

Figure 4. Dielectric relaxation spectra of pure water and ice. The dielectric constant is ϵ'/ϵ_0, and the dielectric loss is ϵ''/ϵ_0.

where σ is the low-frequency conductivity in mhos per meter. At a frequency of about 10^8 Hz, ϵ''/ϵ_0 passes through a minimum as the loss caused by dipole rotations becomes important. When salts are added to the water, an ionic conduction increases the dielectric loss. The influence of salts on the dielectric properties of water decreases with increasing frequency and is small at frequencies higher than 10^{10} Hz.

The dielectric relaxation spectra of ice given in Figure 4 show that ice is a low loss dielectric at ultra-high frequencies and microwave frequencies. High-frequency measurements on ice [10^{10} Hz (Lamb and Turney 1949)] yielded a value of 3.05 for ϵ'/ϵ_0 and no observable change occurred in this value over the temperature range 0° to -40°C.

The loss tangent of ice measured at a frequency of 10^{10} Hz is given as a function of temperature in Figure 5. If the loss tangent at 10^{10} Hz were caused only by the component resulting from the absorption at 10^4 Hz, then the loss tangent would be derived from:

$$\tan \delta = \frac{(\epsilon'_s - \epsilon'_\infty)}{\epsilon'_\infty \omega \tau} .$$

At $\omega = 2\pi \times 10^{10}$ radians/sec and -5°C this yielded a value of 0.17×10^{-4} for tan δ. The measured loss tangent under these conditions was 0.45×10^{-3}, or about 27 times larger than the calculated value. This discrepancy was probably caused by a frequency-dependent conductivity term. The large values of tan δ are mainly observed in polycrystalline ice.

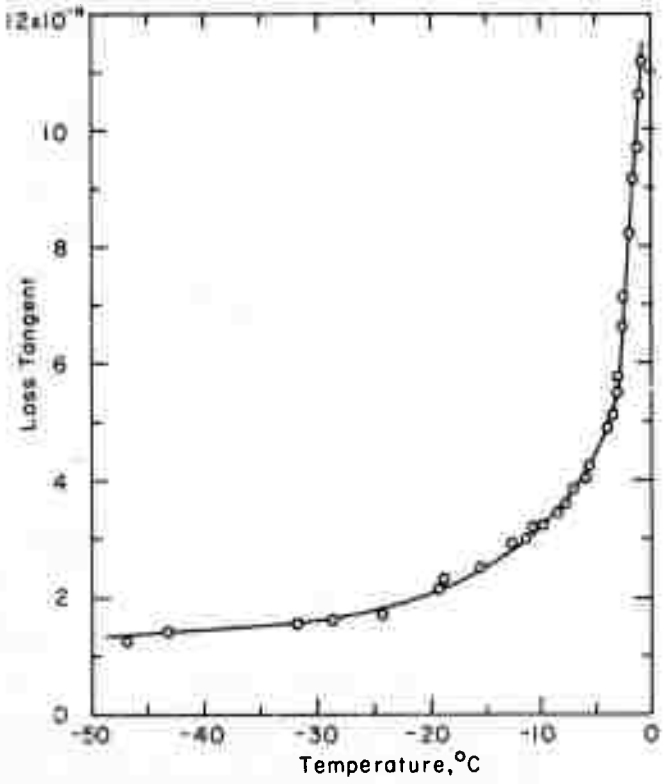

Figure 5. The loss tangent of ice samples as a function of temperature at a frequency of 10^{10} Hz (Lamb and Turney 1949). (Copyright, The Institute of Physics, Bristol, England; reprinted by permission.)

Dielectric properties of snow

Snow is a mixed dielectric of ice and air; therefore, the dielectric constant and dielectric loss are related to the density of the snow. Measurements made by Cummings (1952) on the relative dielectric constant of snow as a function of density at a frequency of 9.4×10^9 Hz (*X*-band radar) are given in Figure 6. These data follow the mixture formula

$$\frac{\epsilon'_m - 1}{3\epsilon'_m} = \nu \frac{\epsilon'_i - 1}{\epsilon'_i + 2\epsilon'_m}$$

where ν is the volume fraction of ice and the subscripts m and i refer to the snow and solid ice respectively. The dielectric loss of snow is also strongly temperature dependent. Figure 7 (Cummings 1952) gives the loss tangent of snow samples of various densities as a function of temperature at a frequency of 9.4×10^9 Hz. Measurements on cores of snow of relatively high densities from Greenland and Antarctica were made at the Laboratory of Insulation Research, Massachusetts Institute of Technology (Waite 1965); these are given in Figure 8.

Because of the large differences between the dielectric properties of ice and those of water, the dielectric behavior of a snow cover is strongly dependent on the free water content of the snow. Cummings (1952) measured the loss tangent of snow as a function of the free water content at a frequency of 9.4×10^9 Hz. Figure 9 shows that small percentages of water drastically increase the loss tangent of snow. The dielectric properties of snow cover can thus be expected to show large variations at temperatures near 0°C. The dependence of free water in snow covers on environmental parameters such as temperature and age is not well documented.

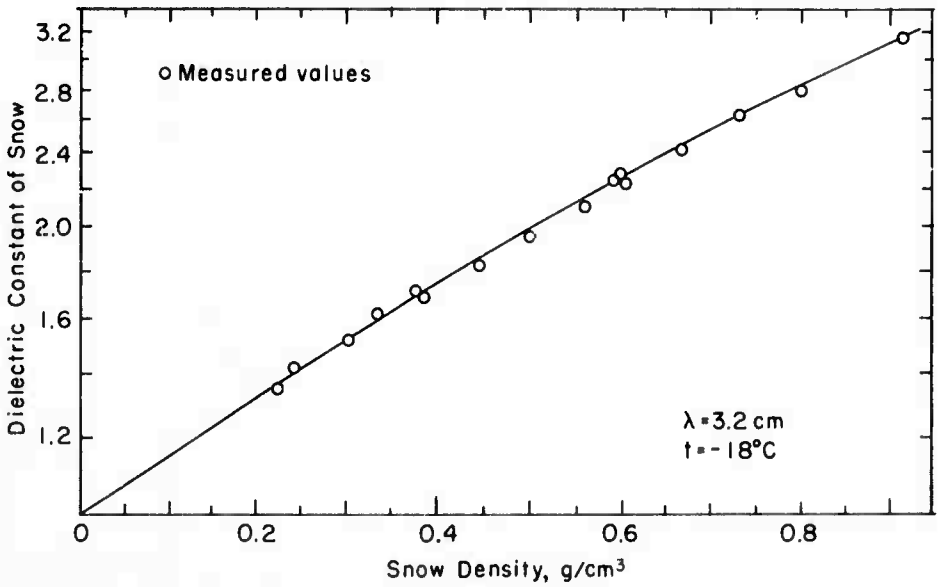

Figure 6. The relative dielectric constant of snow as a function of density at a frequency of 9.4×10^9 Hz (Cummings 1952). (Copyright, Journal of Applied Physics, American Institute of Physics; reprinted by permission.)

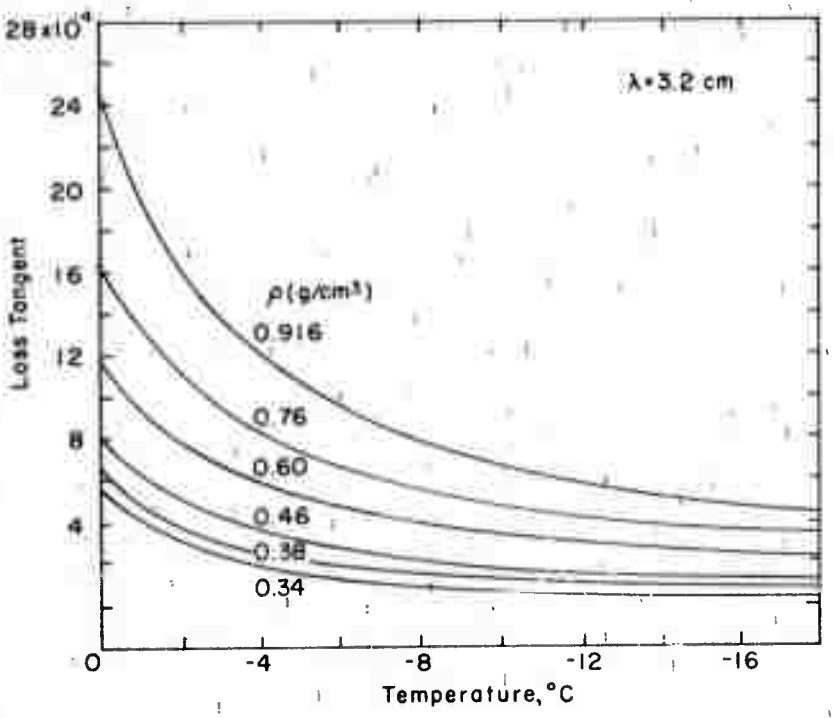

Figure 7. The loss tangent of snow as a function of temperature at a frequency of 9.4 × 10⁹ Hz (Cummings 1952). (Copyright, Journal of Applied Physics, American Institute of Physics; reprinted by permission.)

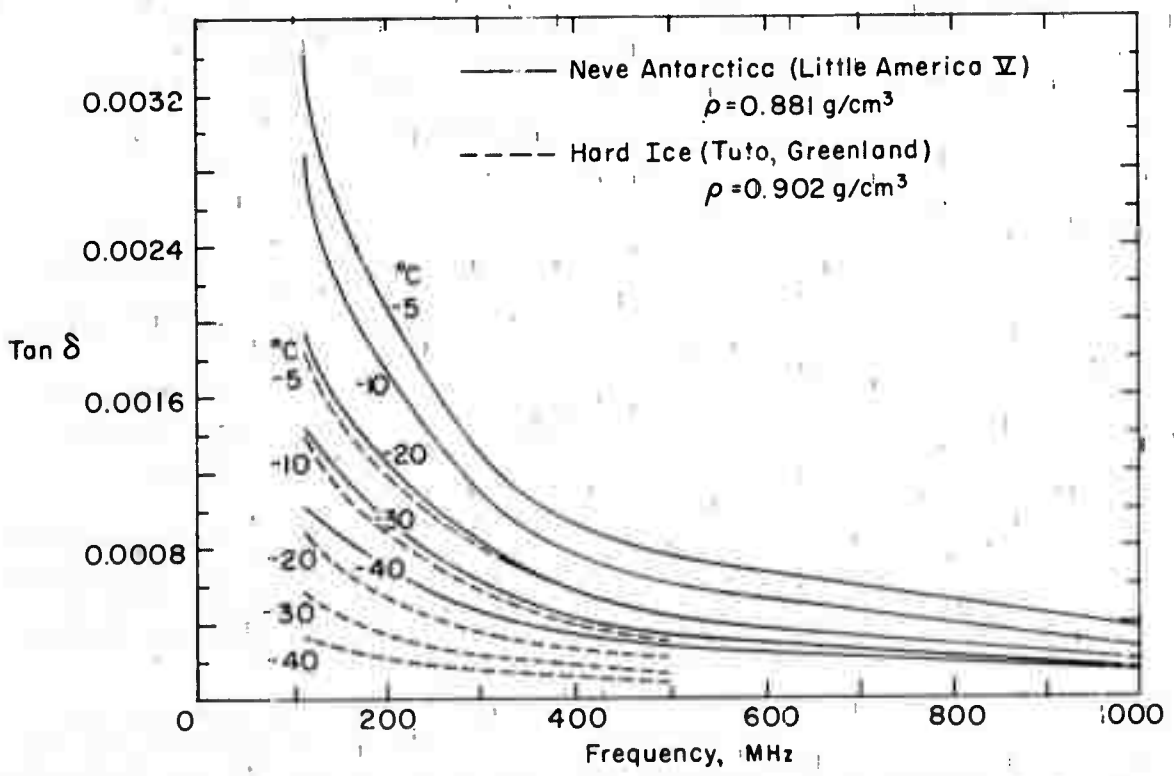

Figure 8. The loss tangent of snow cores from Greenland and Antarctica at several temperatures as a function of frequency (Waite 1965).

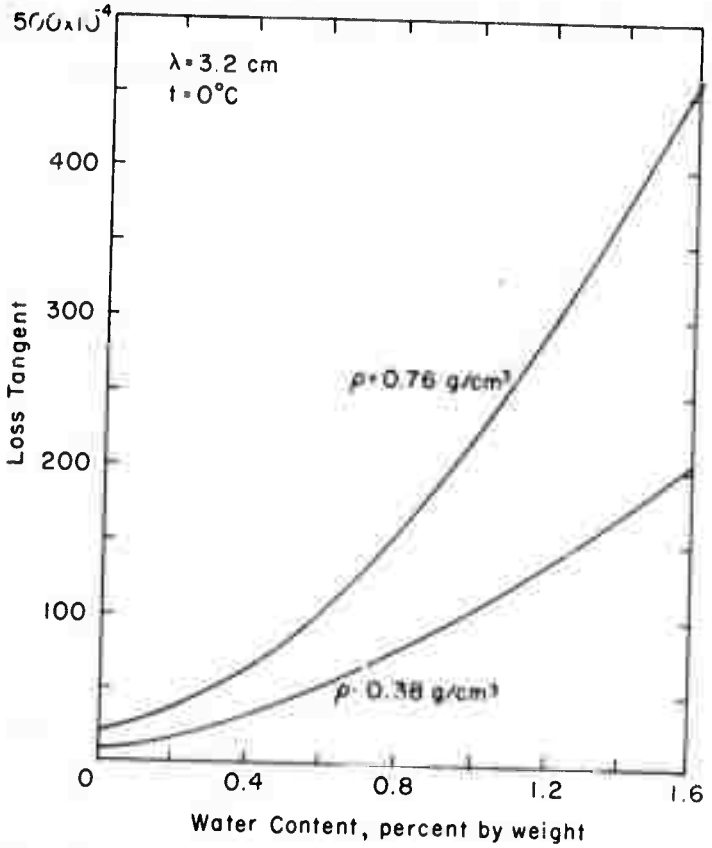

Figure 9. The effect of free water on the loss tangent of wet snow at a frequency of 9.4 × 10^9 Hz (Cummings 1952). (Copyright, Journal of Applied Physics, American Institute of Physics; reprinted by permission.)

Dielectric properties of sea ice

Because liquid inclusions of brine are entrapped in its ice matrix, sea ice differs from fresh-water ice in physical behavior. This difference is strongly evident in the dielectric properties of the two ice forms (Hoekstra and Cappillino 1971). The amount of brine entrapped in the ice depends on the rate of ice growth, and for young sea ice it may reach salinities as high as 20 parts per thousand. The brine pockets are not stationary once the ice has formed. Under the influence of gravity brine drainage occurs through interconnecting channels in the sea ice matrix, and under the influence of temperature gradients brine pockets diffuse through the ice to the warm side of the ice (Lofgren and Weeks 1969).

Since the dielectric properties of water are strongly frequency dependent in the frequency range 10^9 Hz to 10^{11} Hz, the dielectric properties of sea ice, because of the presence of liquid inclusion, are also strongly frequency dependent. In Figure 10 the dielectric loss of sea ice is plotted as a function of frequency (Hoekstra and Cappillino 1971). Sea ice at microwave frequencies is thus a *medium* loss dielectric, whereas fresh-water ice is a *low* loss dielectric.

Furthermore, because the amount of liquid water in sea ice changes with temperature, the dielectric properties of sea ice are strongly temperature dependent. This is shown in Figures 11a and b, which give the dielectric properties of sea ice as a function of temperature at a *K*-band and an *X*-band frequency respectively.

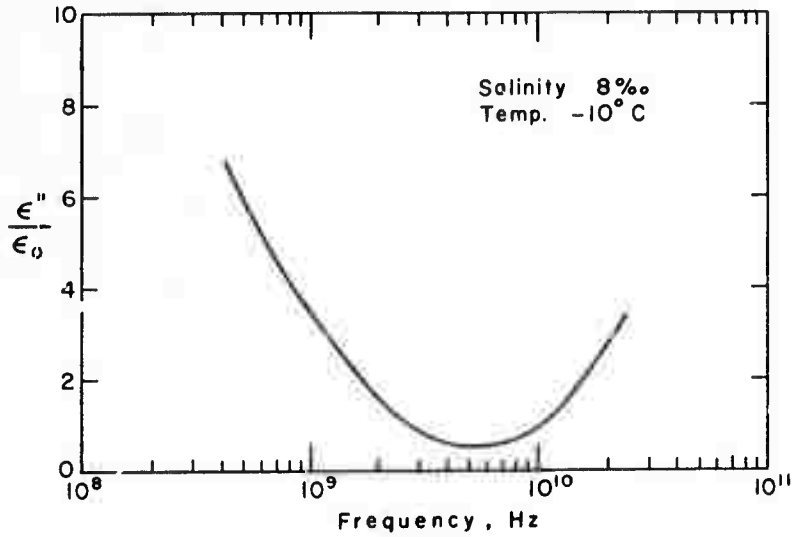

Figure 10. The dielectric loss of sea ice as a function of frequency (Hoekstra and Cappillino 1971).

Sea ice thus differs from fresh-water ice in its dielectric behavior at microwave frequencies in that 1) it has a dielectric loss 3 to 4 orders of magnitude larger than that of fresh-water ice; and 2) its dielectric properties, both the dielectric constant and the dielectric loss, are strongly temperature dependent, whereas the dielectric constant of fresh-water ice is only slightly temperature dependent.

Reflection of electromagnetic waves from air on snow and ice at VHF and microwave frequencies

The reflection coefficients discussed here are those relating to the incidence of plane waves at plane surfaces. The reflection coefficient depends on the angle of incidence, the dielectric properties of the media, the polarization of the incident radiation and the thickness of the snow cover.

In general, a wave on reflection changes in both amplitude and phase, so that the reflection coefficient R is of the form

$$R = |R| e^{j\psi}$$

where ψ is the advance in phase after reflection. Saxton (1950) considered the case illustrated in Figure 12. The incident ray on encountering the snow surface is partially reflected (Ray 1) and refracted (Ray 2). The refracted wave undergoes further refractions and reflections at the boundary of Media B and C. Medium C may be water or land. It is assumed that the refracted wave continues in Medium C without further reflections. By a series of multiple reflections, Ray 3, Ray 4, etc. refract from the snow back into free space and superpose with Ray 1. The superposition of Ray 1, Ray 2, etc. causes a dependence of the reflection coefficient of the snow on the thickness of the snow cover. Saxton (1950) computed these changes in reflection with snow thickness for a lossless snow at several angles of incidence. His results are given in Figure 13. The snow thickness t is given as the number of free-space wavelengths t/λ. The reflection coefficient changes considerably with snow thickness. Figure 14 gives the amplitude of reflection coefficient when no multiple reflections occur.

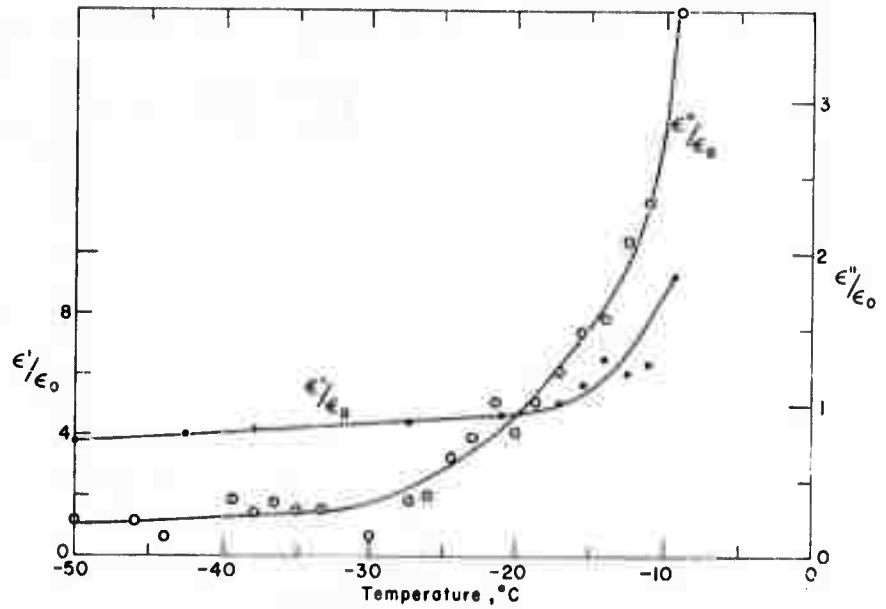

a. *At a frequency of* 2.3×10^{10} *Hz (K-band).*

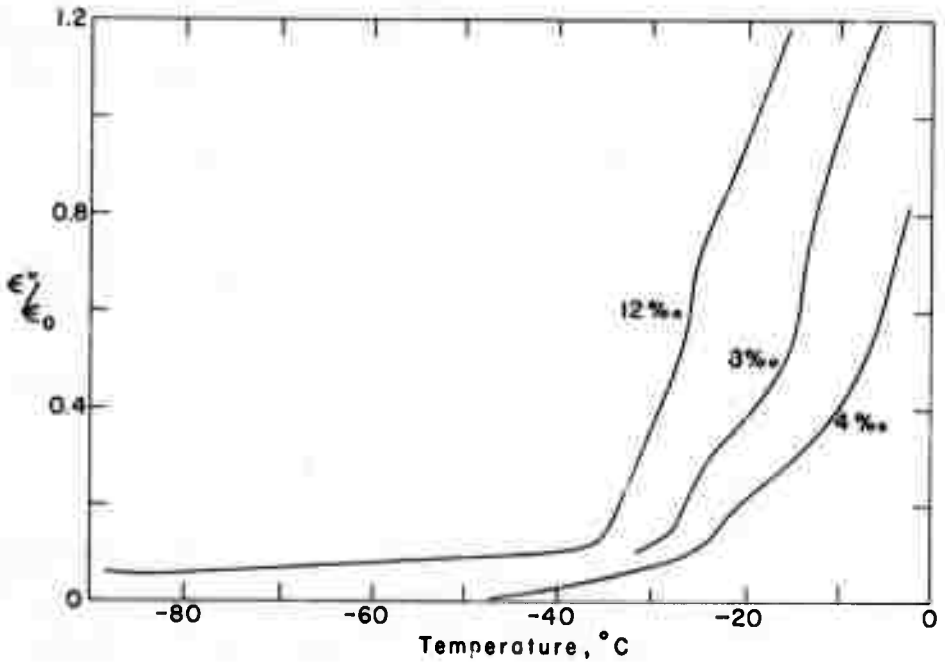

b. *At a frequency of* 10^{10} *Hz (X-band) and several salinities in parts per thousand.*

Figure 11. The dielectric properties of sea ice as a function of temperature.

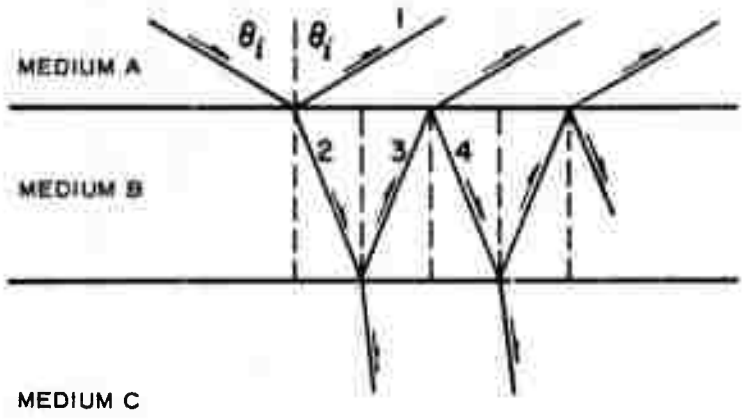

Figure 12. Schematic diagram of multiple reflections and refractions taking place in a snow layer over land or ice surfaces.

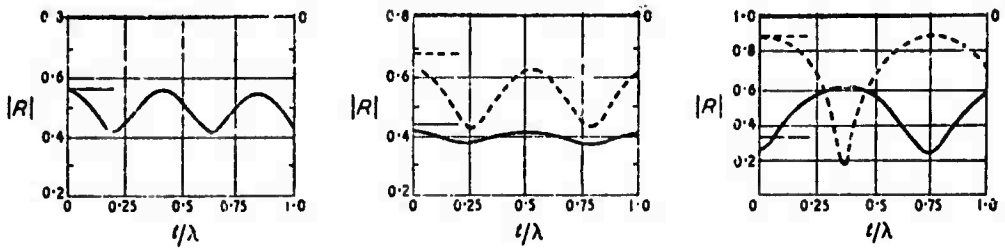

a. *Angle of incidence = 0° (normal incidence).*

b. *Angle of incidence = 45°.*

c. *Angle of incidence = 80°.*

Figure 13. The computed amplitude of the reflection coefficient of snow ($\epsilon'/\epsilon_0 = 1.4$) as a function of snow thickness t/λ (Saxton 1950). The dotted lines are for horizontal polarization and the solid lines are for vertical polarization. (Copyright, IPC Electrical-Electronic Press Ltd; reprinted by permission.)

As the angle of incidence approaches 90° (grazing incidence) the effects of multiple reflections must become increasingly less significant, because the reflection coefficient of the boundary between Medium A and Medium B approaches unity for both types of polarization. In Figure 15 the amplitude of reflection coefficients is computed at an angle of incidence of 89° with and without multiple reflections. The maximum variation in reflection coefficient caused by multiple reflections is 0.82 to 0.98 at horizontal polarization.

The computations that led to the results given in Figures 14 and 15 neglected the effect of absorption in the snow cover. When the snow contains free water, the influence of the thickness of the snow cover can be expected to decrease rapidly because of the attenuation of the radiation.

Suzuki and Hasegawa (1958) determined the reflection coefficient at 4 GHz by probing the vertical field pattern of a horn antenna. They measured the reflection coefficient on natural snow from January through March 1955. During this period the temperature, and thus the loss tangent of the snow, changed probably by an order of magnitude (0.011 – 0.1). Figure 16 gives the amplitude

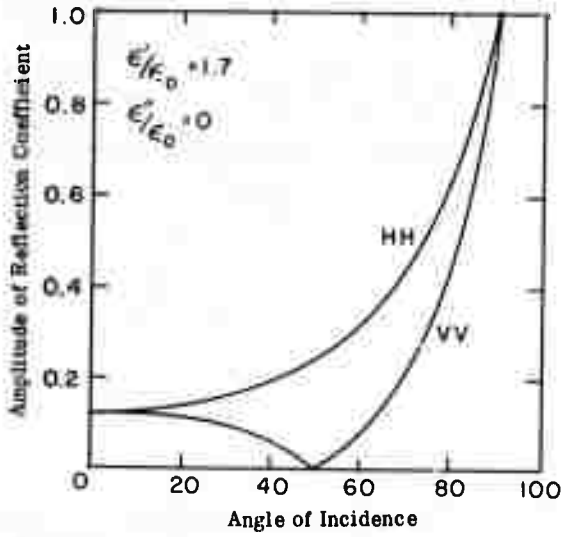

Figure 14. The computed amplitude of reflection coefficient from a snow surface as a function of angle of incidence. For vertical and horizontal polarization.

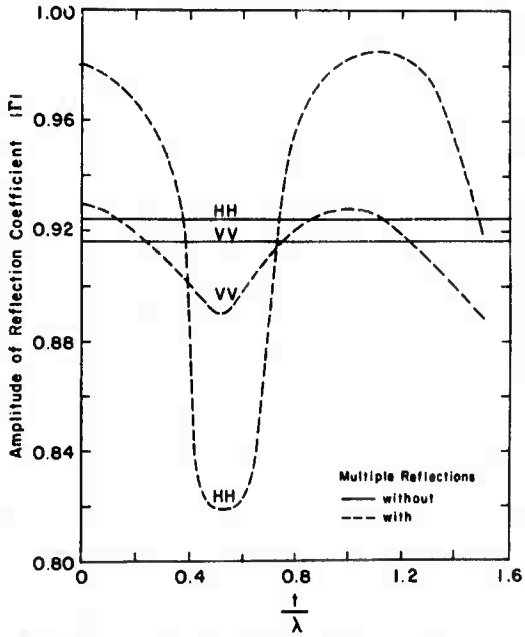

Figure 15. The amplitude of reflection coefficient at an angle of incidence of 89° for snow ($\epsilon'/\epsilon_0 = 1.2$) computed with and without multiple reflections. The thickness of the snow is given in number of free space wavelengths

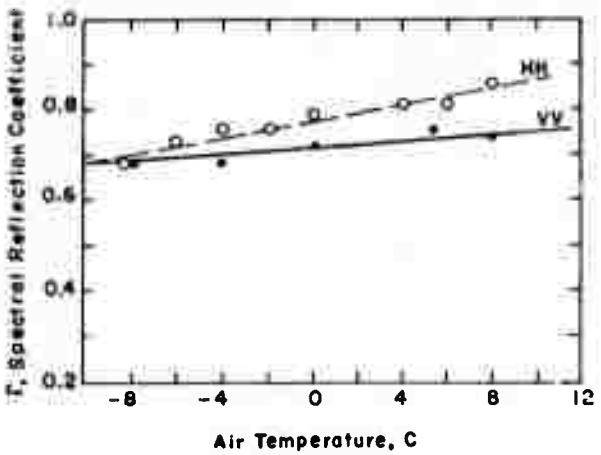

Figure 16. The amplitude of reflection coefficient of natural snow surfaces as a function of air temperature at a grazing angle of 2° 15' and a frequency of 4 GHz (after Suzuki and Hasegawa 1958).

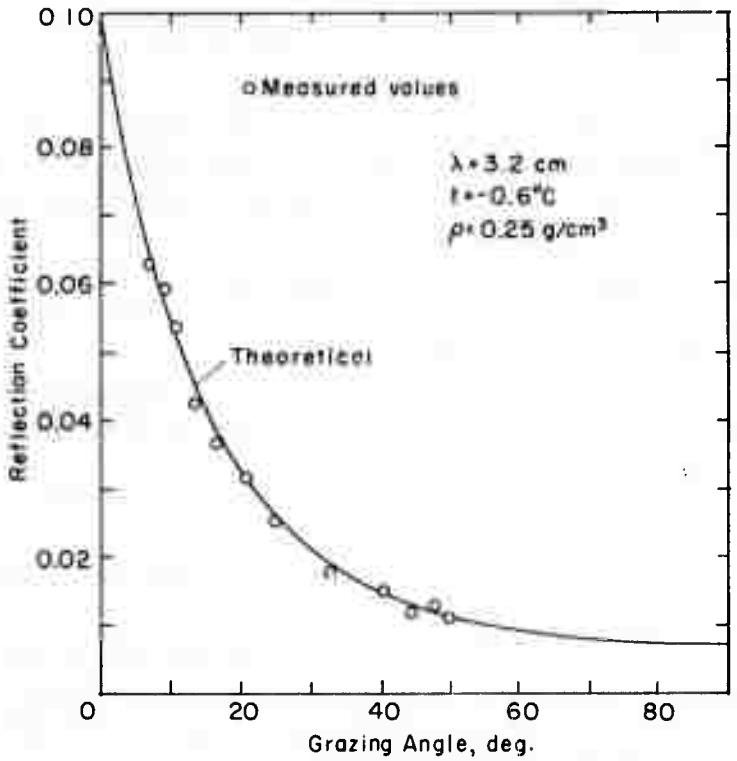

Figure 17. Measured and theoretical reflection coefficients of a sand surface covered with 10 in. of snow at several grazing angles (Cummings 1952). (Copyright, Journal of Applied Physics, American Institute of Physics; reprinted by permission.)

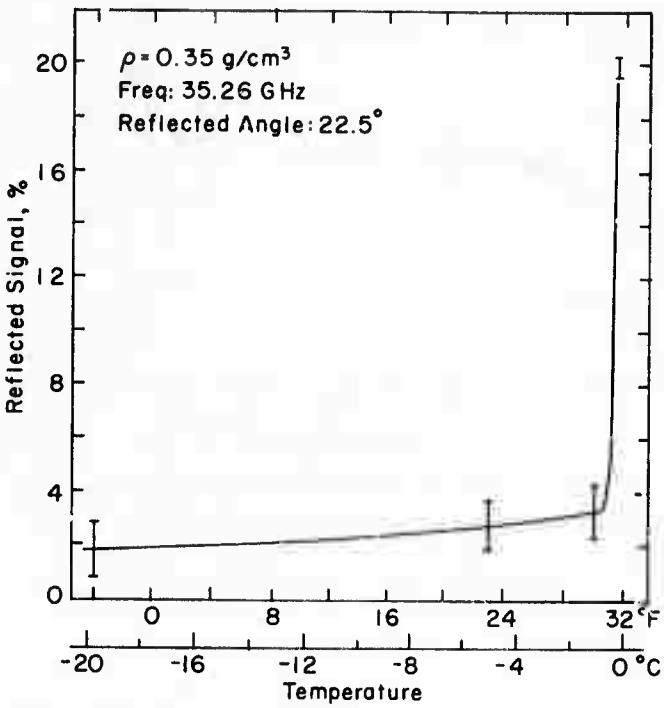

Figure 18. Measured reflection signal of snow as a function of temperature at a frequency of 35.26 GHz and a grazing angle of 67.5° (Battles and Crane 1966).

of reflection coefficient measured by Suzuki and Hasegawa (1958) as a function of air temperature. A difference of several degrees between snow temperature and air temperature is expected. The reflection coefficient increases when the snow warms. The increase is substantially higher for horizontally polarized radiation than for vertically polarized radiation.

Cummings (1952) experimentally measured the reflection coefficient from snow surfaces overlying sand surfaces. His results (Fig. 17) show no evidence of multiple reflection and compare very well with theoretical data, assuming reflection from the snow surface only.

Reflections from snow surfaces were also measured at the *K*a-band frequency by Battles and Crane (1966) at a 22.5° angle of incidence. The percentage of the reflected signal is given in Figure 18 as a function of temperature. These data again point out the great importance of the free-water content on the dielectric properties of snow. It seems likely that at temperatures above 30°F some free water is present in the snow.

Two discrepancies, therefore, must be resolved to provide an understanding of the reflection from snow surfaces.

1) Theoretically, multiple reflections are expected from dry snow overlying land and water surfaces (Saxton 1950). On the other hand, the experimentally measured reflection coefficients of snow overlying sand show no evidence of multiple reflections (Cummings 1952) and behave as if the reflection takes place from an infinitely thick snow layer.

2) At low grazing angles (< 2°), where the influence of dielectric loss on the reflection coefficient is, theoretically, expected to be negligible, measurements of Suzuki and Hasegawa (1958) showed a strong dependence of the reflection coefficient on the snow temperature.

EQUIPMENT PARAMETERS

10-GHz radar equipment parameters

Transmitter. The 10-GHz transmitter is a pulsed TWT radar system with a peak power output of 1 kw. The pulse rate is adjustable from 500 Hz to 5000 kHz, and the pulse width from 0.1 to 0.5 μsec. One-kHz pulse rate and 0.125-μsec pulse width were used for most measurements at Post Pond. The first side lobes of the antenna (frequency spectrum) were maintained 10 db below the main lobe to ensure a high-quality pulse shape.

Receiver. The receiver consists of mixer, local oscillator, pre-intermediate-frequency (PRE-IF) amplifier, intermediate-frequency (IF) range gating circuits, and video detector. In the radat target scattering (RATSCAT) system, a unique system is used for precision amplitude measurements. A 60-MHz stable reference pulse is generated between transmitter pulses. This pulse is routed through a precision mechanical attenuator controlled by a mechanical servo, and is then injected into the

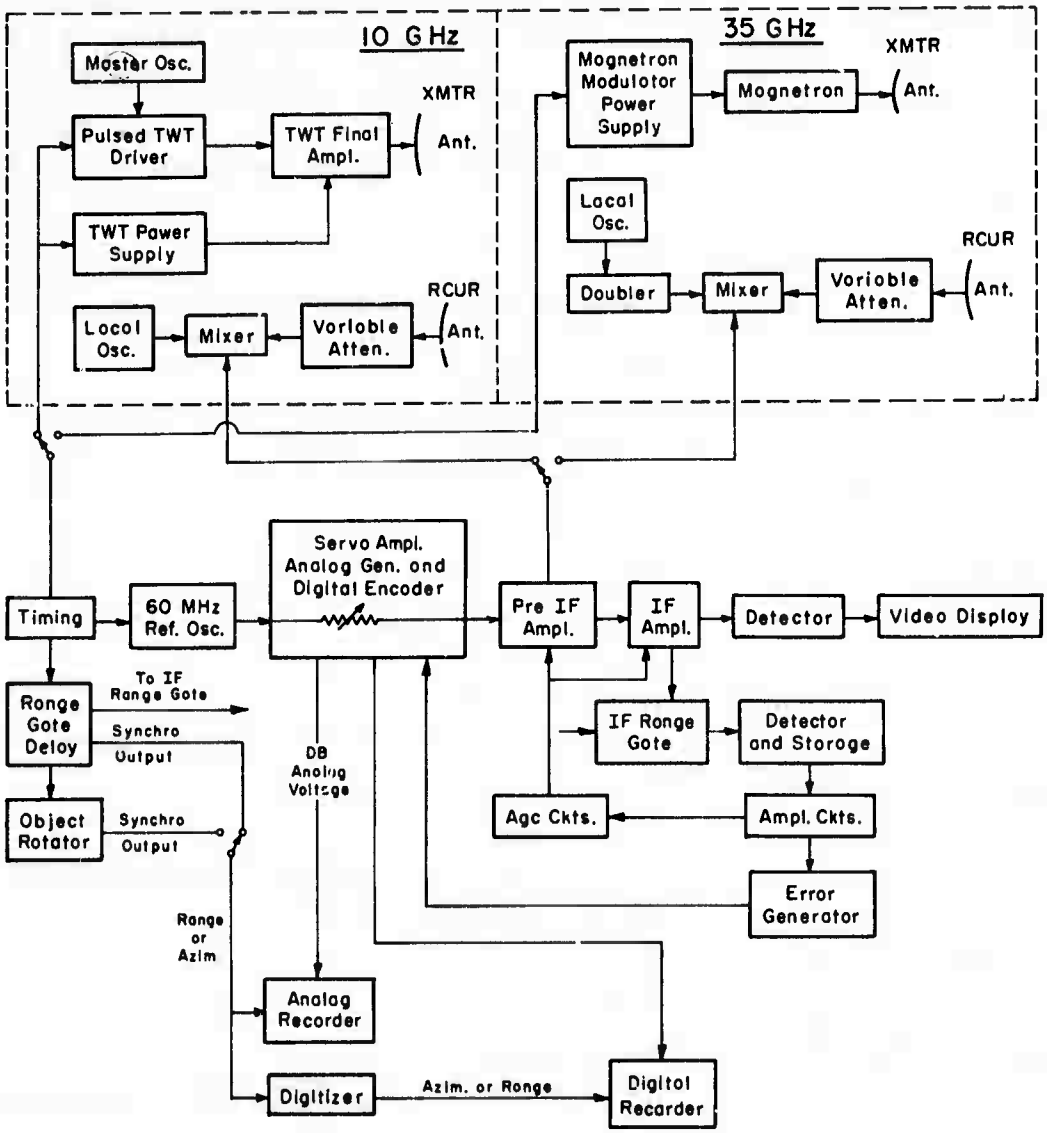

Figure 19. Circuit diagram of the 10-GHz and 35-GHz radars.

receiver PRE-IF amplifier at the same location as is the mixer output. The range gated reference pulse and target pulse are processed to develop an error signal to drive the servo for zero error. In this manner, the attenuation of the mechanical attenuator is related to the received power. Since both the mixer output and the reference pulse are processed through the IF and video circuits, nonlinearities and drift from these circuits are not reflected in the data output. System stability and linearity are thus determined by transmitter power output stability and mixer linearity. Setup of the equipment ensures that the mixer is not used in the nonlinear range (above –20 db for the *X*-band system). A circuit diagram of this equipment is given in Figure 19.

Video processing. The information output of the RATSCAT system consists of analog voltages, digitized output of range (0 to 3600 ft), and received signal power (0 to 50.0 db). Range information reflects the center position of the video range gate from the radar antennas in feet.

In the cross section of ice objects at a fixed place, the range information is replaced by the azimuth position of the target rotator (in degrees).

Antennas and antenna structures. Two 6-ft-diam parabolic dishes were used in the *X*-band system, thus avoiding system recovery problems and the inherent losses associated with circulator and radio frequency (RF) switching circuits. The 6-ft antennas were mounted on a movable platform with 7.0 ft between their centers. The entire assembly was moved up or down to achieve the desired antenna heights for the measurements. A flexible waveguide was used to reduce the time associated with changing antenna heights. Antenna pattern plots were made for the 6-ft antennas. The 3-db beamwidths measured are listed in Table I; Table I also lists the important parameters of the *X*-band radar system.

Table I. Parameters of 10-GHz radar system.

Frequency	10 GHz ± 10 MHz
Power output	1 kw nominal (peak)
Pulse width	0.125 μsec (σ^0 measurements) 0.2 μsec (rotating object measurements)
Pulse repetition frequency	1.0 kHz
Receiver minimum detectable signal	–94 dbm
Receiver bandwidth	10 MHz
IF frequency	60 MHz
Range gate width	0.1 μsec
Dynamic range	50 db
Linearity	± 0.5 db
Equipment stability	0.1 db/hr avg 0.25 db/hr worst case
Antenna types	6-ft-diam parabolic reflector with horn or circular polarization feeds
Antenna horizontal beamwidth (measured)	Vertical polarization, 1.33° Horizontal polarization, 1.27° Circular polarization, 1.06°
Polarizations	Any combination of linear polarization or transmit-right-circular and receive-left-circular polarization
Range gate position resolution	1 ft
Range accuracy	± 10 ft
System recovery from transmitter Pulse or large object return	0.5 μsec max
Data format: analog	50-db signal return vs 3600-ft range
or	50-db signal return vs 360.0° azimuth rotation
digital	Digital output on paper tape of range and signal return every 4 ft
Range gate/detector characteristics	Sample and hold peak IF signal occurring during range-gate duration (0.1 μsec)

35-GHz radar equipment parameters

Transmitter. The 35-GHz transmitter is a pulsed magnetron system using a NARDA-type 10010 modulator and power supply. The magnetron is a SFD type 330 having approximately 10-kw peak power output.

Receiver. The receiver consists of a local oscillator (17.5 GHz) and a passive frequency doubler driving a balanced mixer using IN53M-R diodes. The mixer output is interfaced directly with the RATSCAT system.

Video processing. Same as that of 10-GHz system.

Antennas. Two 1-ft-diam Scientific Atlanta parabolic dishes (Model S/A-22-1) and associated feeds are mounted on 2-ft centers. The antennas are located as close as practical to the transmitter and receiver to reduce waveguide losses. Table II gives the important parameters of the 35-GHz radar system. Figure 19 gives a circuit diagram of this system.

Table II. Parameters of 35-GHz radar system.

Frequency	About 35 GHz
Power output	About 10-kw peak
Pulse width used	0.15 to 0.2 μsec, depending on waveguide length and VSWR
Equipment stability	2.0 db per 8-hr measurement series, maximum (measured)
Antenna type	S/A type 22-1; 1-ft-diam parabolic reflector with associated horn feeds
Polarizations	Any combination of linear polarizations
System recovery from transmitter pulse or large object return	1.0 μsec maximum
Other	See Figure 19.

95-GHz radar equipment parameters

The 95-GHz system is a monostatic radar. This radar system consists of transmitter, duplexing device, receiver, mixers, antenna, trigger generator, local oscillator, power supplies, display, and controls. Pertinent parameters are listed in Table III.

Antenna (transmitter and receiver). The antenna consists of a 24-in.-diam parabolic dish that has a gain of about 53 db and a beamwidth of 0.38° at half-power points. A Cassegrain feed is used. The table on which the antenna is mounted allows a 60° horizontal scan and a 30° vertical scan. The antenna table can be manually controlled or servo-driven on both axes.

Duplexing system. The duplexing system determines the closest range at which meaningful data can be taken. The ferrite circulator has a maximum isolation of 20 db between the input port and the mixer port, and this amount of isolation is insufficient to protect the crystal mixer from burnout during the transmitting pulse. To provide additional attenuation for the leakage signal during the transmitting pulse, a ferrite switch is inserted between the circulator and the crystal mixer. The ferrite switch is a driven device that has 45-db attenuation when there is no current flow; this reduces the leakage signal enough to protect the mixer. The insertion loss of the circulator and the ferrite switch during minimum attenuation is 4 db. The ferrite switch is triggered by the same modulator as the magnetron, and the ferrite switch is thus triggered during the start of the outgoing pulse. The duration of the pulse is 0.1 μsec. The response time of the switch is 1 μsec.

Table III. Parameters of 95-GHz radar system.

Transmitter	
Frequency	95.5 GHz
Peak power output	4 kw
Pulse repetition frequency	1500 pps
Pulse length	0.1 sec
Average power	0.6 w
Receiver-balanced mixer	
Intermediate frequency	60 MHz
Bandwidth	40 MHz
Antenna	
Beamwidth	0.38°
Gain	53 db

Transmitter. A type DX-287 Amperex magnetron is used. The pulse repetition frequency is 1500 pps, the pulse length 0.1 μsec, the average power output 0.6 w, and the peak power output 4 kw. The primary power supply for the high voltage source is 115 v at 400 Hz, 3 phase.

MEASUREMENT AND CALIBRATION

10- and 35-GHz radar systems

To interpret usefully the data on backscatter from ice obstacles and snow surfaces the data must be calibrated in such a manner that a cross section per unit area σ^0 independent of the radar parameters can be determined. The radar cross section of ground clutter was obtained by comparing the clutter signal with the return from a calibration target. The calibration target was a metal sphere placed in the first lobe of the ground-plane effective antenna pattern (Fig. 20). This method was used because of the physical problems of locating a calibration standard high enough to avoid the energy reflected from the ground. The following discussion develops the theory and method used to calibrate the 10-GHz and 35-GHz radar systems and the method used to determine σ^0 from the recorded data.

Energy reflected from the ground is used effectively on a ground-plane radar range when the target to be measured is placed at the point in space where the reflected signal and direct signal add in phase. This addition occurs in both the transmitted signal and the received signal. If the amplitude of the voltage of the reflection coefficient of the ground plane is $|\Gamma|$, then at the point where the direct beam from the transmitter and the reflected beam add in phase, the total voltage is.

$$E_t = E_d(1 + |\Gamma|) \tag{1}$$

where

E_t = total voltage at target

E_d = voltage at target caused by direct wave only.

The reflected signal at the receiver antenna is similarly given by

$$E_r = E_b(1 + |\Gamma|) \tag{2}$$

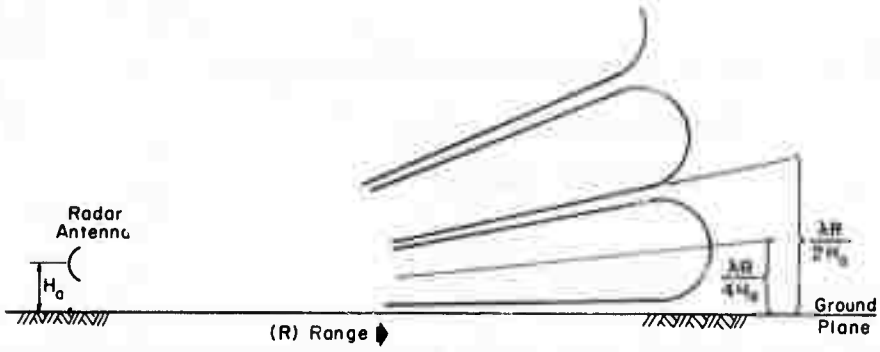

Figure 20. The vertical field pattern of an electromagnetic wave propagating over a plane reflecting surface. R = range, H_a = antenna height, λ = wavelength.

where

E_r = total voltage at receiver antenna

E_b = voltage at antenna caused by direct backscatter energy.

The power received at the antenna from a radar target positioned at the proper point in space (where energy of direct and reflected waves adds in phase) is $(1 + |\Gamma|)^4$ larger than the power received if the target were in free space at the same range. The classic radar range equation can be rewritten to represent the ground-plane situation as follows:

$$S_f = \frac{\sigma G^2 \lambda^2 P_t}{(4\pi)^3 R^4} \tag{3}$$

$$S_g = \frac{\sigma G^2 \lambda^2 P_t}{(4\pi)^3 R^4} (1 + |\Gamma|)^4 \tag{4}$$

where

S_f = signal received from a target in free space (w)

σ = cross section of target (m^2)

λ = wavelength (m)

P_t = transmitted power (w)

G = antenna gain (dimensionless)

R = range to target (m)

S_g = signal received from a target located in center of first ground-plane lobe (w).

Calibration of the system is accomplished by obtaining a return for a calibration target in the ground plane at a predetermined range.

$$S_{gcal} = \frac{\sigma_{cal} G^2 \lambda^2 P_t (1 + |\Gamma|)^4}{R_{cal}^4 (4\pi)^3} = \sigma_{cal} \left(\frac{1 + |\Gamma|}{R_{cal}} \right)^4 K \tag{5}$$

where

S_{gcal} = signal from ground-plane calibration target (w)

σ_{cal} = cross section of calibration target (m^2)

R_{cal} = range to calibration target (m)

K = calibration constant $\dfrac{G^2 \lambda^2 P_t}{(4\pi)^3}$.

The radar cross section of a target located at range R may be obtained by rearranging eq 3 as follows:

$$\sigma = \frac{(4\pi)^3 R^4 S_f}{G^2 \lambda^2 P_t} = \frac{R^4}{K} S_f = \frac{S_f R^4 \sigma_{cal} (1 + |\Gamma|)^4}{S_{gcal} (R_{cal})^4} \tag{6}$$

where K is substituted from eq 5. For measurements of snow clutter $\sigma_{clutter}$ where a free-space calibration is desired, eq 6 may be expressed as:

$$\sigma_{clutter} = \frac{S_{clutter}}{S_{gcal}} \left(\frac{R_{clutter}}{R_{cal}} \right)^4 (1 + |\Gamma|)^4 \sigma_{cal}. \tag{7}$$

In terms of dbsm, the cross section in db relative to a 1 square meter target becomes:

$$\sigma^{dbsm}_{clutter} = \sigma^{dbsm}_{cal} + 40 \log \left(\frac{R_{clutter}}{R_{cal}} \right) + 40 \log (1 + |\Gamma|) + S^{db}_{clutter} - S^{db}_{gcal}. \tag{8}$$

The accuracy of measurements made on clutter is limited by the ability to measure the range to the clutter (range gate delay), the ability to ensure a ground-plane situation during calibration, the accuracy to which Γ is known, and the stability of the calibration. Calibration stability is about ± 0.5 db. The measurements of range are within ± 10 ft. A calibration range of 1500 ft, therefore, yields an expected error of ± 0.2 db caused by range inaccuracies.

At a 1° grazing angle a value of 0.95 for $|\Gamma|$ is expected; therefore, this value was used in all calculations. An attempt was made to measure Γ by placing a 4-in. metal sphere in both a minimum and a maximum of the effective ground-lobe antenna pattern. The reflection coefficient is related to the signal received at the maximum and minimum by:

$$\frac{(1 + |\Gamma|)^4}{(1 - |\Gamma|)^4} = \frac{S_{max}}{S_{min}}.$$

A separation of 40 db between S_{max} and S_{min} was measured at 10 GHz; this gave a value of $|\Gamma| = 0.82$. However, this represents a lower limit, since the size of the sphere limits the separation that can be obtained. The values measured for $|\Gamma|$ by Suzuki and Hasegawa (1958) at 2° 15' were in the same range, but their data showed large variations with air temperature (Fig. 16). In our calculations a value of 0.95 was used throughout because in the absence of detailed data it was better to adhere to the value calculated from the Fresnel equations. The uncertainty in $|\Gamma|$ could thus introduce a maximum error of –1.5 db. The overall absolute error in measurement of $\sigma_{clutter}$ was estimated to be less than (–1.5 ± 0.7)db.

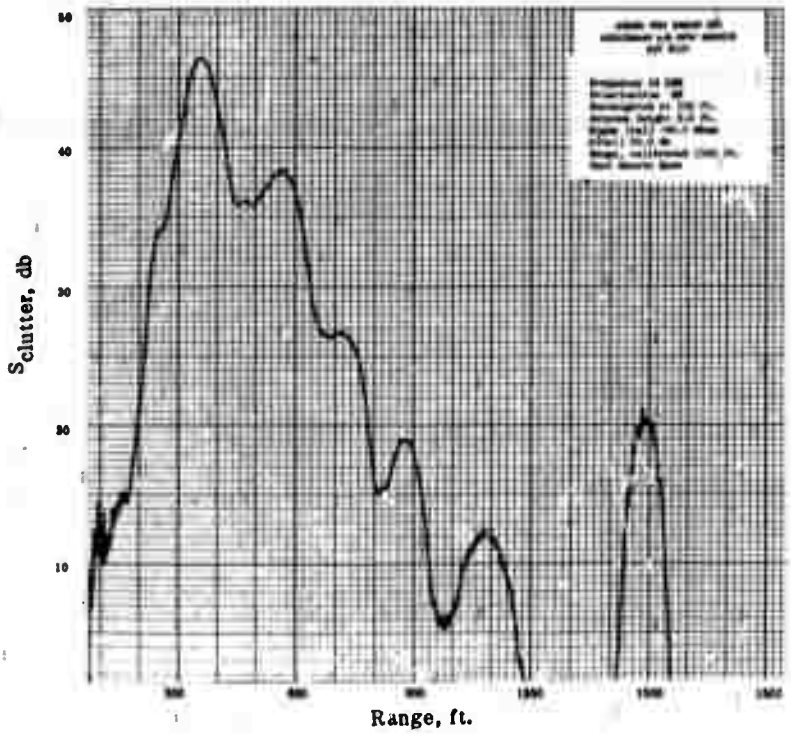

Figure 21. A typical example of an analog plot obtained from ground clutter.

Each measurement series was preceded by a system calibration. After this calibration, the antennas were directed toward the area of interest by temporarily placing an object with a high radar cross section in the center of the area (normally 550 ft in range) and adjusting the antennas for maximum return. The system drift was monitored during a measurement sequence by transferring to a secondary standard for each analog plot. At the end of the measurement sequence the original calibration was checked to verify the stability and accuracy of the calibration (post calibration). Agreement within 0.2 db between the calibration and post calibration was accepted for these measurements.

The data at 10 and 35 GHz consisted of analog photos and digital paper tape of return in db versus range at 4-ft intervals. Figure 21 gives a typical plot of return from an undisturbed snow surface. The target at a range of 1500 ft was the calibration sphere. The digital tapes of radar return versus range were reduced by using eq 8 to find $\sigma^{dbsm}_{clutter}$ versus range. The value of the calibration constant $\sigma^{dbsm}_{cal} - S^{db}_{gcal}$ was recorded for each plot, R_{cal} was 1500 ft, $|\Gamma|$ was taken to be 0.95, and $R_{clutter}$ and $S^{db}_{clutter}$ were obtained from the data plot. The term $\sigma^{dbsm}_{clutter}$ thus obtained was the sum of the returns over the area illuminated by the antenna beam. To find the cross-section characteristics per unit area σ^0

$$\sigma^0 = \frac{\sigma_{clutter}}{A_{eff}}$$

where A_{eff} is the effective area of terrain used in measurements of clutter.

A_{eff} is dependent on:

1) transmitted pulse width (recorded for each measurement)

2) range to target area to be measured (range gate position)

3) antenna radiation pattern.

A_{eff} is thus a function of the radar system. At the very low grazing angles used in these tests, A_{eff} was taken to be:

$$A_{eff} = \frac{c\,\tau\,\theta\,R}{2\sqrt{2}}$$

where

τ = transmitted pulse width

c = velocity of the electromagnetic wave in free space

θ = beamwidth at the 3-db power points

R = range to the area measured.

The $\sqrt{2}$ in the denominator accounts for the variation in power within the 3-db power points. Table IV gives A_{eff} for several configurations used in the tests.

Table IV. A_{eff} for several test configurations.

Frequency (GHz)	*Range (ft)*	θ (°)	*Polarization*	τ *(sec)*	A_{eff} (m^2)
10	550	1.33	HH	0.125	47
10	550	1.27	VV	0.125	45.4
10	550	1.06	CIR	0.125	46.2
35	550	1.90	HH, VV	0.20	120
35	550	1.90	HH, VV	0.19	114
35	550	1.90	HH, VV	0.17	101
95	1070	0.38	HH, VV	0.1	23

95-GHz radar system

Because of the narrow beamwidth of the 95-GHz radar its antenna could be boresighted by a telescope. The antenna was boresighted on a corner reflector placed on a ½-in. wooden rod at a 10-ft height. The return of the corner reflector was obtained by attenuating the return with a precision variable attenuator until it was indistinguishable from system noise. The value of the attenuation was recorded as the decibel return of the corner reflector. Later in the test program, when the 95-GHz system was interfaced with the RATSCAT system, the data were recorded on analog plots.

After the return from the corner reflector was obtained, the antenna was boresighted on the base of the wooden rod on which the corner reflector was mounted. The antenna mount was then displaced successively at 2° intervals of azimuth angle and the data of the return from smooth snow were recorded. The terrain clutter was measured and the measurements were calibrated at a range of 1070 ft. An example of return from the undisturbed snow surface is given in the *A*-scope display of Figure 22.

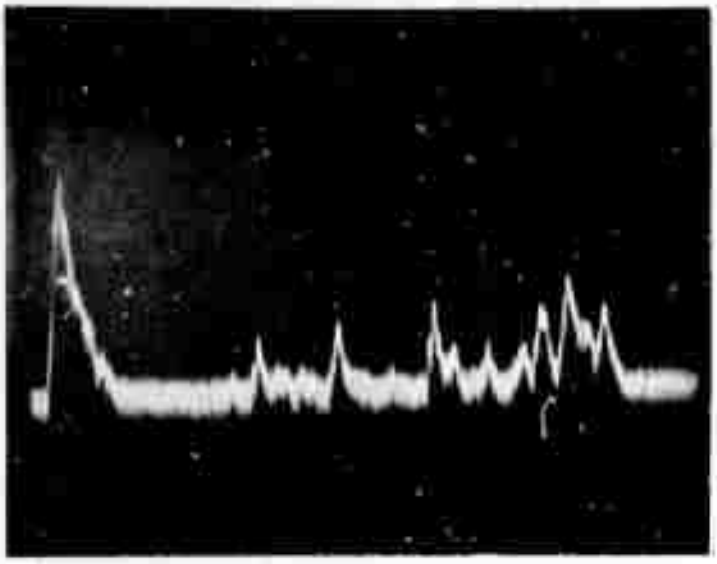

Figure 22. An example of return from an undisturbed snow surface given by an A-scope display of the 95-GHz system.

The data on the ice objects were also obtained 1) by attenuating the returns from the ice objects with a precision variable attenuator until they disappeared into the noise, and 2) by taking the returns from the analog plots (these data were used after the 95-GHz radar was interfaced with the RATSCAT system).

RESULTS AND DISCUSSION

Four types of measurements were made to obtain the environmental parameters for the design of a terrain avoidance radar:

1) The terrain clutter from undisturbed snow surfaces was measured at frequencies of 10, 35 and 95 GHz, at grazing angles of 1° to 0.3°. At 10 GHz the measurements were made at linear, circular and cross polarizations; at 35 GHz, at linear and cross polarizations; and at 95 GHz, at linear polarizations.

2) The terrain clutter from periodically spaced trenches in the snow surface was measured at 10 GHz and 35 GHz, at grazing angles of 1.0, 0.65 and 0.38°, at linear polarizations.

3) The radar cross section of ice blocks placed on the snow surface was obtained at 10, 35 and 95 GHz, at linear and cross polarizations. Blocks of different sizes were used.

4) The free-space radar cross sections of rectangular blocks of fresh-water and salt-water ice were measured by placing the blocks on rotating Styrofoam columns. The cross sections were obtained as a function of aspect angle in the maximum of the first ground lobe antenna pattern.

Returns from undisturbed snow surfaces

To analyze the data of power received versus range the following considerations were made:

1) The closest range at which data can be taken is determined by system recovery, which was determined to be 300 ft in the 10-GHz and 35-GHz systems, and 1000 ft in the 95-GHz system.

2) The greatest distance at which data can be taken is determined by the magnitude of the return. The return falls off as the third power of range, and the criterion adopted was not to use the data if the return was less than 15 db above the noise.

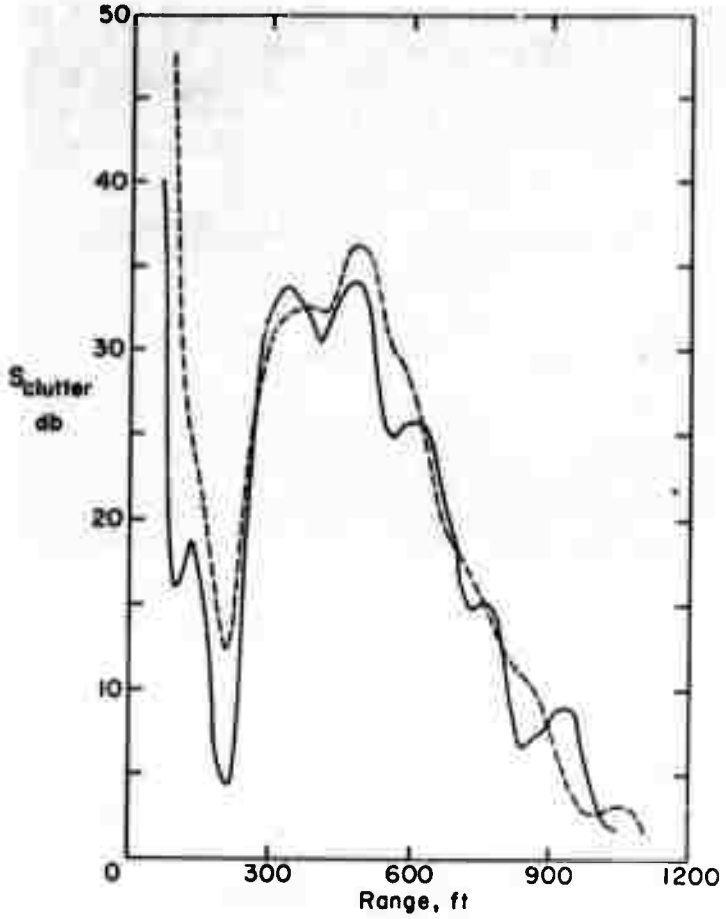

Figure 23. Typical analog plots of the return from smooth snow at 10 GHz and vertical polarization. The solid line represents returns at fixed frequency; the broken line represents returns at 40-MHz simultaneous sweep of transmitter and receiver.

3) Because the return from the snow surface is dependent on the angle of incidence, and the angle dependency measurement of the return was one of the objectives of the program, the return could not be integrated over a large range.

4) The area of integration must lie within the 3-db power points; otherwise a correction for the power variation within the area illuminated by the beam must be made.

To accommodate these considerations the data from 475 to 625 ft were averaged. This area is within the 3-db power points and the angle variation is less than 10 arc sec.

The analog plot of Figure 21 is typical of the data plots obtained at 10 GHz and 35 GHz. There is considerable lobing in the return versus range although no individual targets were evident in the terrain. It was ascertained that the lobing was not caused by side lobes in the antenna patterns by pointing the antenna skywards.

To investigate whether the lobing structure affected the value of σ^0, a swept-frequency experiment was performed. By sweeping the frequency of the transmitter and the receiver 40 MHz simultaneously about the center frequency, the interference patterns of the terrain patches causing the lobing should be destroyed and the return averaged through the lobes. The solid line in Figure 23 is a typical example of the return from a smooth snow surface obtained at fixed frequency; the broken

line represents the return from the same surface at swept frequency. Figure 23 shows that the swept frequency return averages the data through the lobes. Table V compares values of σ^0 obtained at fixed and swept frequencies. In most instances the agreement is within ± 1.5 db. A satisfactory explanation for the lobing, in what appears to be uniform terrain, has not been found. Local differences in the snow profile most likely caused this lobing in the radar return versus range.

Table V. Comparison of the values of σ^0 obtained at fixed and swept frequencies.
The transmitter and receiver were swept at 40 MHz simultaneously about the center frequency.

Center frequency GHz	*Grazing angle (°)*	*Surface condition*	*Polarization*	*Fixed frequency σ^0 (db)*	*Swept frequency 40 MHz σ^0 (db)*
10	1.0	wet snow	VV	–61.4	–61.15
10	1.0	wet snow	HH	–56 4	–55.4
10	1.0	wet snow	HH	–57.9	–56.7
10	1.0	wet snow	HV	–73.1	–71.6
10	1.0	dry snow	HH	–47.4	–45.9
10	0.65	dry snow	HH	–53.2	–52.6
10	0.65	dry snow	VV	–56.5	–52.7
10	0.38	dry snow	HH	–61.4	–58.8
10	0.38	dry snow	VV	–63.7	–62.1
10	0.38	dry snow	HV	–78.7	–80.6

Figures 24a-e give σ^0 in db as a function of grazing angle for several polarizations at 10 GHz. Figure 25a and b give similar data at 35 GHz. During the measurement period of the data shown in Figures 24a-d the temperatures of the surface layer of snow did not rise above 0°C, so the snow was dry. The density of the snow over the lake ice varied from 0.08 to 0.2 g/cm^3 and the depth of snow from 0 to 12 in. The measurements were repeatable; thus the depth and density of dry snow do not measurably affect the radar backscatter at low angles of incidence.

In the second week of February a warm period occurred, the air temperature rose above 0°C, and a light rain fell for a short period. The snow cover then contained free water. The radar backscatter decreased by approximately 10 db. The results are given in Figure 26 as a function of time and in Figure 27 as a function of snow temperature. When the air temperature dropped and the snow again became dry, the radar backscatter increased to previous values.

The presence of small amounts of free water in the snow drastically affects the loss tangent of the snow (Cunnings 1952), and Suzuki and Hasegawa (1958) showed that the reflection coefficient at low grazing angles increases substantially when the snow warms up. The temperature dependence of the backscatter and the reflection coefficient is probably caused by penetration of the refracted wave in the dry snow cover and subsequent reflection and backscatter from lower layers, such as the lake ice surface. Because of the higher dielectric constants of the underlying media, the refracted wave bends towards the normal, and backscatter takes place at higher grazing angles. The value of σ^0 normally increases with increasing angle of incidence. If the snow were wet, the wave would be rapidly attenuated with depth, and the backscatter from the top surface would be expected to dominate.

Tables VIa and b give the values of $\sigma^{\text{dbsm}}_{\text{clutter}}$ measured at 95 GHz for horizontally and vertically polarized radiation respectively at a range of 1070 ft and at 2° azimuth intervals. Azimuth of 0° was taken to be at the base of the pole on which the corner reflector was mounted. The antenna mount was rotated to the same settings several times. The grazing angle of these measurements was 0.3°.

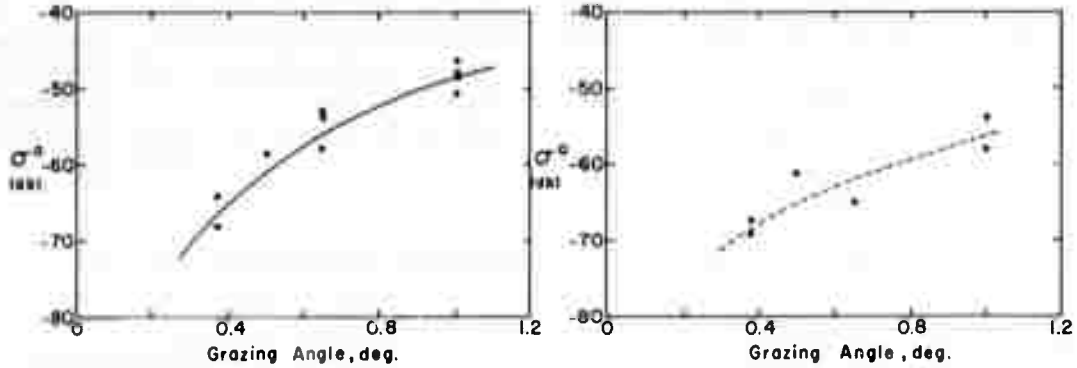

a. *Horizontal polarization.* b. *Vertical polarization.*

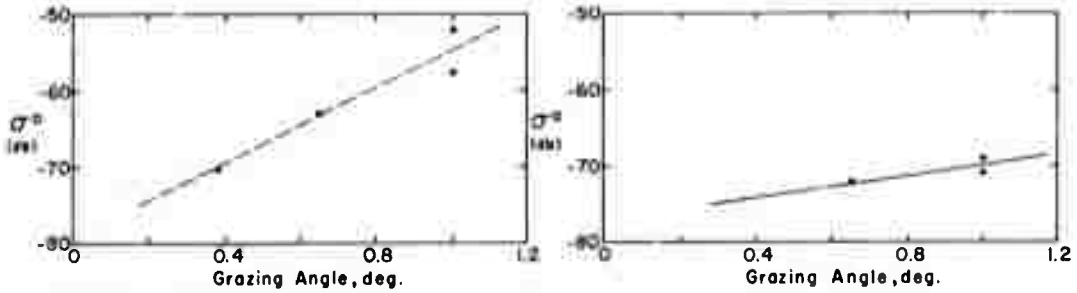

c. *Circular polarization (some sense of rotation).* d. *Cross polarization.*

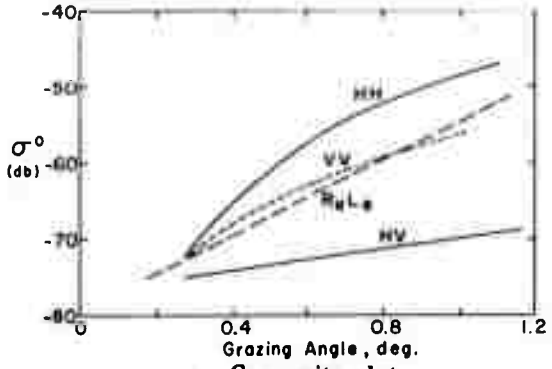

e. *Composite plot.*

Figure 24. Measured values of σ^0 from undisturbed snow surfaces as a function of grazing angle at a frequency of 10 GHz.

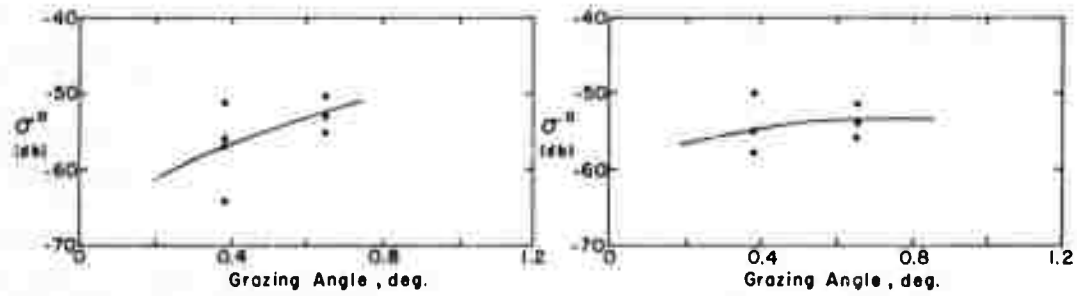

a. *Horizontal polarization.* b. *Vertical polarization.*

Figure 25. Measured values of σ^0 from undisturbed snow surfaces as a function of grazing angle at a frequency of 35 GHz.

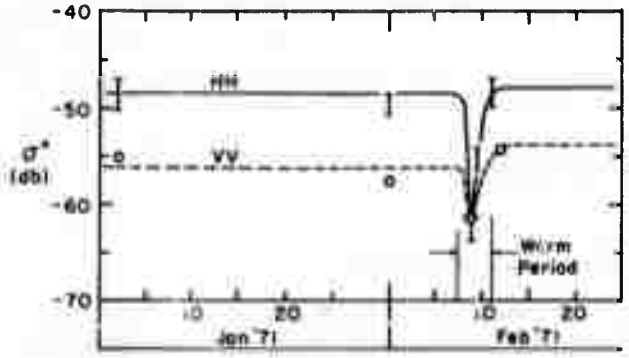

Figure 26. Variation of σ^0 from undisturbed snow surfaces with time at a frequency of 10 GHz. For horizontal and vertical polarization.

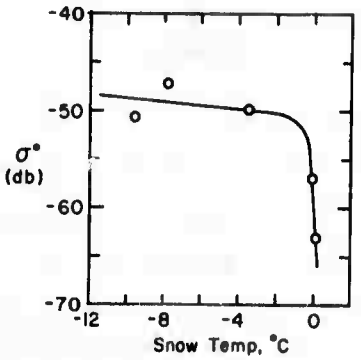

Figure 27. Variation of σ^0 as a function of snow temperature at 10 GHz and horizontal polarization.

Table VIa. $\sigma^{dbsm}_{clutter}$ at 95 GHz at a range of 1070 ft obtained at 2° azimuth intervals for horizontally polarized radiation.

Azimuth 0° was taken to be at the base of the wooden pole on which the corner reflector was mounted.

Azimuth angle (°)	$\sigma^{dbsm}_{clutter}$			
0	–23	–24	–21	–19
2	–15	–22	–21	–14
4	–17	– 7	– 2	–14
6	–19	–25	–23	–16
8	–12	– 9	0	– 5
10	–29	–35	–33	–37
12	–29	–38	–40	–36
14	–33	–34	–34	–30
16	–34	–35	–36	–35
18	–30	–31	–31	–30
20	–35	–35	–34	–34
22	–38	–35	–34	–34
24	–26	–30	–34	–29

Table VIb. $\sigma^{dbsm}_{clutter}$ at 95 GHz at a range of 1070 ft obtained at 2° azimuth intervals for vertically polarized radiation.

Azimuth of 0° was taken to be at the base of the wooden pole on which the corner reflector was mounted.

Azimuth angle (°)	$\sigma^{dbsm}_{clutter}$			
0	–19	–17	–20	–20
2	–16	–23	–17	–17
4	–26	–22	–17	–12
6	–23	–19	–23	–18
8	–13	–27	–23	–15
10	–41	–41	–35	–37
12	–41	–41	–41	–38
14	–41	–41	–37	–37
16	–36	–41	–37	–32
18	–32	–38	–34	–33

The value of $\sigma^{dbsm}_{clutter}$ varied from 0 dbsm to –41 dbsm. Such a large variation precludes a meaningful averaging of $\sigma^{dbsm}_{clutter}$. The 95-GHz radar evidently distinguishes local roughnesses (targets) in the terrain.

Effects of surface roughness on σ^0

The effect of the roughness of the terrain on σ^0 depends on the orientation, distribution, height and periodicity of the roughness. The effect of the height of the roughness is often expressed in terms of the Rayleigh criterion. A surface is considered smooth for

$$h < \frac{\lambda}{8 \cos \theta_i}$$

where

λ = wavelength of the radiation in free space

h = height of the disturbance

θ_i = angle of incidence of the electromagnetic plane wave.

Table VII gives the value of h in the Rayleigh criterion for several test conditions. At 10 GHz relatively high obstacles are required before they can be expected to affect σ^0; on the other hand, obstacles 2 or 3 cm high may affect σ^0 at 95 GHz.

Table VII. The value of h in the Rayleigh criterion for roughness $h < \lambda/8 \cos \theta_i$ for several test conditions.

Frequency (GHz)	λ *(cm)*	θ_i	h *(cm)*
10	3	1	22
10	3	0.5	43
35	0.86	1	6.3
35	0.86	0.5	12.3
95	0.31	1	2.3
95	0.31	0.5	4.4

Disturbances in the smooth surface were made by a snow blower. When these experiments were performed, the snow depth over the ice was 8 in. The snow blower cleared the snow down to the ice, resulting in trenches with vertical walls, 2 ft wide and 8 in. deep. The distance between the trenches was varied from 20 ft to 5 ft. The direction of the trenches was perpendicular to the radar beam. The prepared area was made sufficiently large so that illumination by the radar fell well within the area.

The values of σ^0 measured on the disturbed snow surface at 10 GHz and 35 GHz are given in Tables VIIIa and b. At 10 GHz, the value of σ^0 was not measurably influenced by the trenches in the snow, until the trenches were spaced at 5 ft. At 35 GHz, σ^0 increased gradually when the spacing between the trenches was decreased.

Table VIIIa. Effect of disturbances in smooth snow on σ^0 at 10 GHz.

Spacing between steps	*Frequency (GHz)*	*Polarization*	*Grazing angle (°)* 0.38	0.65	1.0
Smooth	10	HH	−67	−57	−49
20	10	HH		−58	−52
10	10	HH	−67	−61	−53
5	10	HH	−60	−53	−47
Smooth	10	VV	−68	−62	−57
20	10	VV		−62	−54
10	10	VV	−63	−54	−56
5	10	VV	−61	−53	−46

Table VIIIb. Effect of disturbances in smooth snow on σ^0 at 35 GHz.

Spacing between steps	*Frequency (GHz)*	*Polarization*	*Grazing angle 0.65°*
Smooth	35	HH	–52
20	35	HH	–50
10	35	HH	–49
5	35	HH	
Smooth	35	VV	–54
20	35	VV	–51
10	35	VV	–38
5	35	VV	

Returns from ice blocks placed on the snow surface

The returns from ice blocks placed on the snow surface at a range of 800 ft were calibrated against a calibration sphere (–20.9 dbsm) placed at a range of 1500 ft. The antenna height used in these experiments was 6.25 ft. The approximately vertical faces of the blocks were oriented perpendicular to the radar beam. Figure 28 shows that the ice blocks did not have perfectly flat surfaces. The smaller blocks were only roughly rectangular since they were shaped by breaking the larger blocks.

The measurements represent the backscatter characteristics of smooth snow and the ice objects. In most instances the ice block returns were considerably higher than the terrain returns, thus making the contribution to $\sigma^{\text{dbsm}}_{\text{clutter}}$ from the terrain negligible. Tables IXa and b give the returns from ice blocks on the snow surface at 10 GHz and 35 GHz respectively. The results are plotted as a function of the sizes of the blocks in Figure 29a and b.

Figure 28. Ice blocks placed on snow surface.

Table IXa. Returns from ice blocks placed on the snow surface at a range of 800 ft with the 10-GHz radar.

Dimensions of ice block (in.)	*Area facing radar (m^2)*	*Polarization*	σ^{dbsm} *ice block*
42 × 22	0.596	HH	15.
21 × 22	0.298	HH	−13.
22 × 10	0.142	HH	−18.
15 × 10	0.0967	HH	−8.
8 × 10	0.052	HH	−7.
42 × 22	0.596	VV	16.
21 × 22	0.298	VV	−11.
22 × 10	0.142	VV	−29.
15 × 10	0.0967	VV	−8.
8 × 10	0.052	VV	−8.
42 × 22	0.596	HV	−2.
21 × 22	0.298	HV	−25.
22 × 10	0.142	HV	−75.
15 × 10	0.0967	HV	−75.
8 × 10	0.052	HV	−67.

Table IXb. Returns from ice blocks placed on the snow surface at a range of 800 ft with the 35-GHz radar.

Dimensions of ice block (in.)	*Area facing radar (m^2)*	*Polarization*	σ^{dbsm} *ice block*
42 × 21	0.57	VV	26.
21 × 21	0.284	VV	14.
10 × 21	0.135	VV	6.
21 × 10	0.135	VV	2.
14 × 10	0.0902	VV	−6.
8 × 10	0.052	VV	−15.
5 × 5	0.016	VV	−16.
42 × 21	0.57	HH	26.
21 × 21	0.284	HH	15.
10 × 21	0.135	HH	6.
21 × 10	0.135	HH	3.
14 × 10	0.0902	HH	−7.
8 × 10	0.052	HH	−4.
5 × 5	0.016	HH	−16.
42 × 21	0.57	HV	16.
21 × 21	0.284	HV	0.
10 × 21	0.135	HV	−9.
21 × 10	0.135	HV	−12.
14 × 10	0.0902	HV	−26.
8 × 10	0.0502	HV	−14.
5 × 5	0.016	HV	−35.

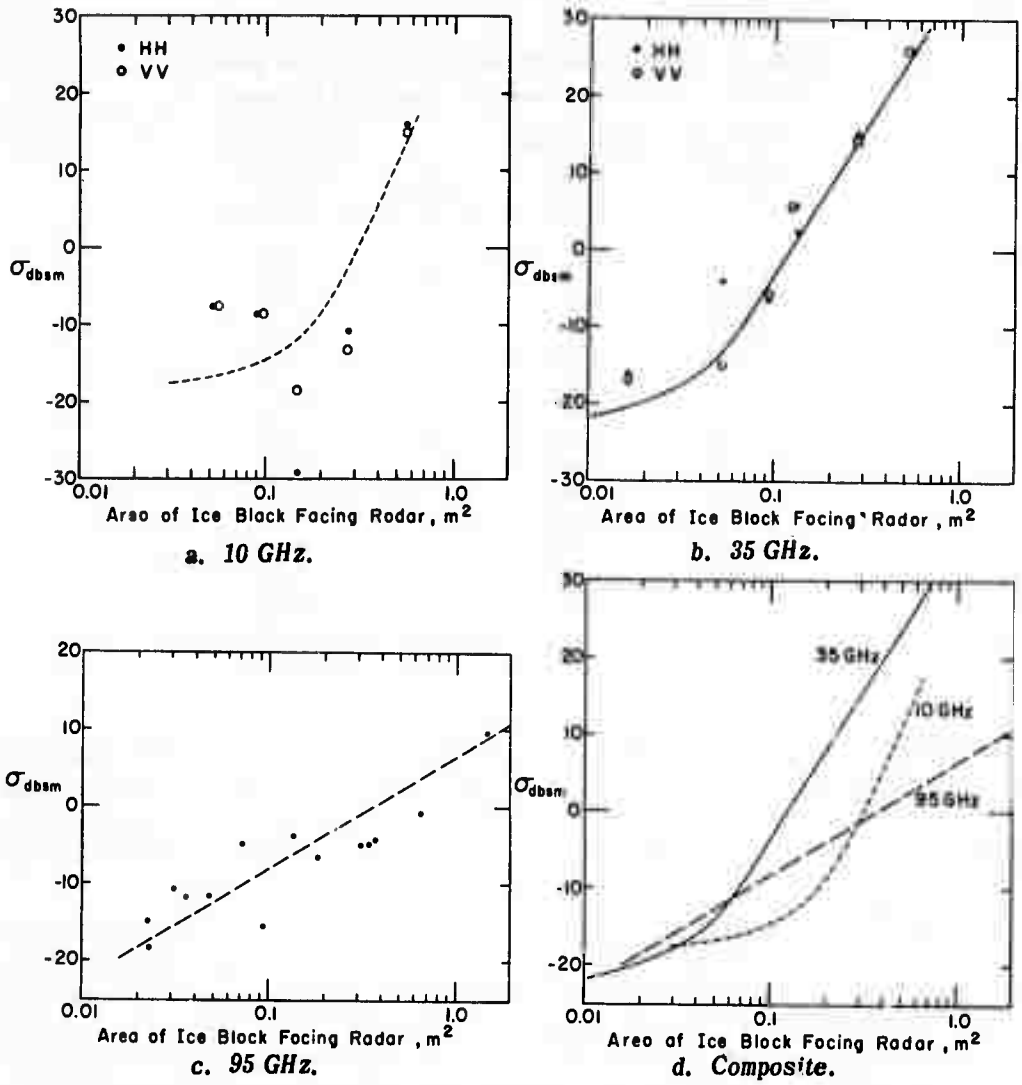

Figure 29. Radar returns from ice blocks placed on snow surface versus area of the blocks facing the radar.

The returns from the ice blocks on the snow surface at 95 GHz were obtained at a range of 1070 ft and calibrated with a corner reflector at the same range. The results are given in Table X and in Figure 29c. Figure 29d gives a composite plot of the returns from the ice blocks at the three frequencies used versus the area of the blocks facing the radar.

The radar returns from large flat plates of arbitrary shapes perpendicular to the radar beam are given by:

$$\sigma^{dbsm} = 10 \log \frac{4\pi}{\lambda^2} + 20 \log A$$

where

λ = free-space wavelength (m)

A = area of ice block facing radar (m^2).

Table X. Returns from ice blocks placed on the snow surface at 95 GHz for vertically polarized radiation.

Dimensions ice block (m)	*Area facing radar (m^2)*	*σ (dbsm)*	*Radar cross section (m^2)*
48 × 48	1.49	+ 9	7.95
24 × 48	0.74	− 2	0.63
24 × 24	0.37	− 4	0.40
12 × 24	0.186	− 7	0.20
12 × 12	0.093	−16	0.025
12 × 6	0.047	−12	0.063
6 × 8	0.035	−12	0.063
6 × 6	0.023	−18	0.016
21 × 48	0.645	− 1	0.80
21 × 24	0.323	− 5	0.31
20 × 10	0.135	− 4	0.40
10 × 10	0.065	− 5	0.31
8 × 8	0.041	−12	0.063
5 × 7	0.0225	−15	0.032
8 × 8	0.041	−11	0.080

For a 10-in. by 10-in. (0.065 m^2) perfectly reflecting plate, values of 17.7, 28.5 and 50 dbsm were expected at 10, 35 and 95 GHz respectively. The radar cross section of carefully planed blocks of ice (placed upon Styrofoam columns) was also measured in free space. The power reflection coefficients of the ice blocks measured in free space varied from 0.005 to 0.08 at 10 GHz and from 0.009 to 0.031 at 35 GHz.

The returns from ice blocks on the snow may, therefore, be expected to be approximately 20 dbsm lower than those from a perfectly reflecting surface, and the cross section is expected to increase with the square of the area. This is approximately the case for the return at 10 GHz and 35 GHz. At 95 GHz the return is 40-50 dbsm lower than calculated and the return increases linearly with area. The backscatter cross section increases linearly when the target becomes a diffuse reflector. Apparently the surface roughnesses of the ice blocks are sufficient for this to happen at 3-mm wavelength.

Returns from ice objects placed on rotator

In this series of tests ice blocks and ice spheres were mounted on Styrofoam columns on a rotator at a range of about 1500 ft (Fig. 30). The returns from the ice blocks were calibrated with a metal sphere placed on the same Styrofoam column. The returns from both the ice blocks and the metal sphere were measured in the first lobe of the ground-plane antenna pattern.

Two ice blocks were made for radar cross-section measurements. One was made from pure ice (formed of distilled water) and one from sea ice (formed of frozen sea water). These blocks were shaped on a band saw to 10 in. × 10 in. × 5 in. The corners of each block were square and the surfaces were smooth.

In addition to the cross-section measurements of the ice blocks, measurements were made of targets consisting of ice blocks and a 10 × 10-in. flat metal plate secured against one 10-in. × 10-in. face of the ice block. The flat plate was positioned broadside toward the radar at an azimuth angle of 180°. The data were recorded on analog plots. Typical analog plots are given in Figures 31a-d.

Figure 30. Metal sphere placed on Styrofoam column on a rotator.

The lobing structures observed for the blocks of ice are typical of those normally obtained when objects are rotated. For flat plates, for example, the nulls between the lobes are separated by an angle α related to the dimension of a rectangular plate by

$$\alpha = \frac{\lambda}{2L} \text{ radians}$$

where L is the length of the plate and λ the wavelength of the radiation.

In general, the pattern of the 10 × 10 × 5-in. ice block consisted of maxima when the flat sides of the block were facing the radar. The blocks were positioned in such a way that the maxima occurred at 0°, 90°, 180° and 270°. Since the radar cross section is a measure of the power reflected in the direction of the radar, the radar cross section depends on the reflection coefficient of the surface facing the ice block. The reflection coefficient is the superposition of two reflected waves, one from the front surface and one from the back surface (assuming that no internal reflections occur). The reflection coefficient is, therefore, a function of the thickness of the block.

Since the radar cross section is proportional to the reflection coefficients at the surfaces of the block, the power reflection coefficients can be calculated by

$$R = \frac{\text{power returned from ice block face}}{\text{power returned from metal plate}}.$$

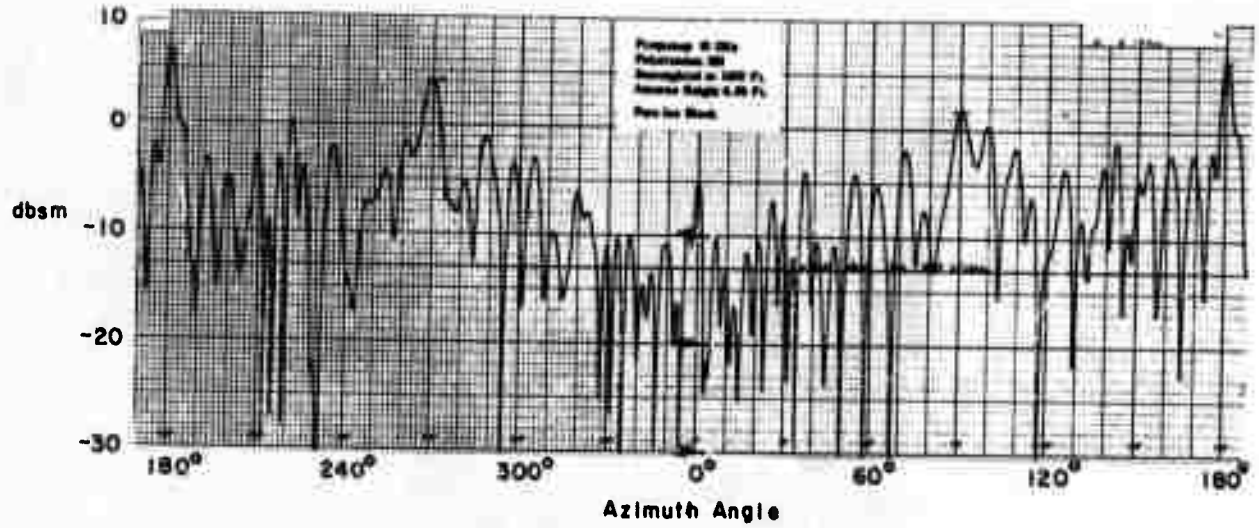

a. Block of pure fresh-water ice.

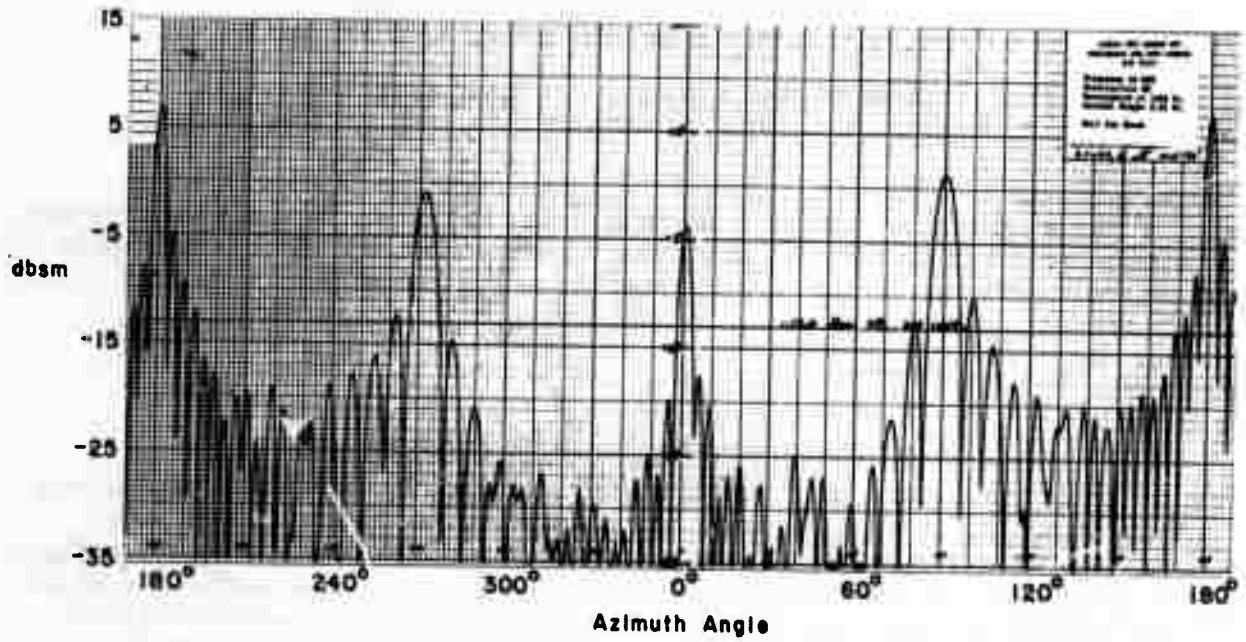

b. Block of salt-water ice.

Figure 31. Analog plots of return in dbsm from 10- × 10- × 5-in. ice blocks placed on Styrofoam column on a rotator as a function of azimuth angle.

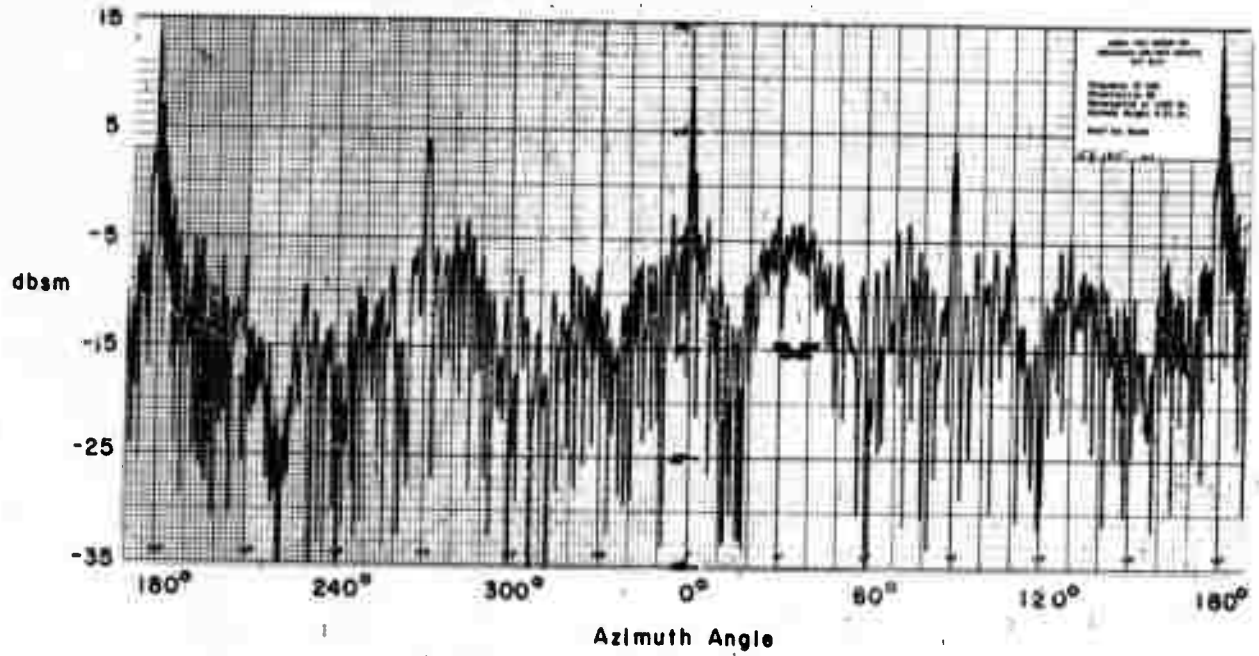

c. Block of pure fresh-water ice.

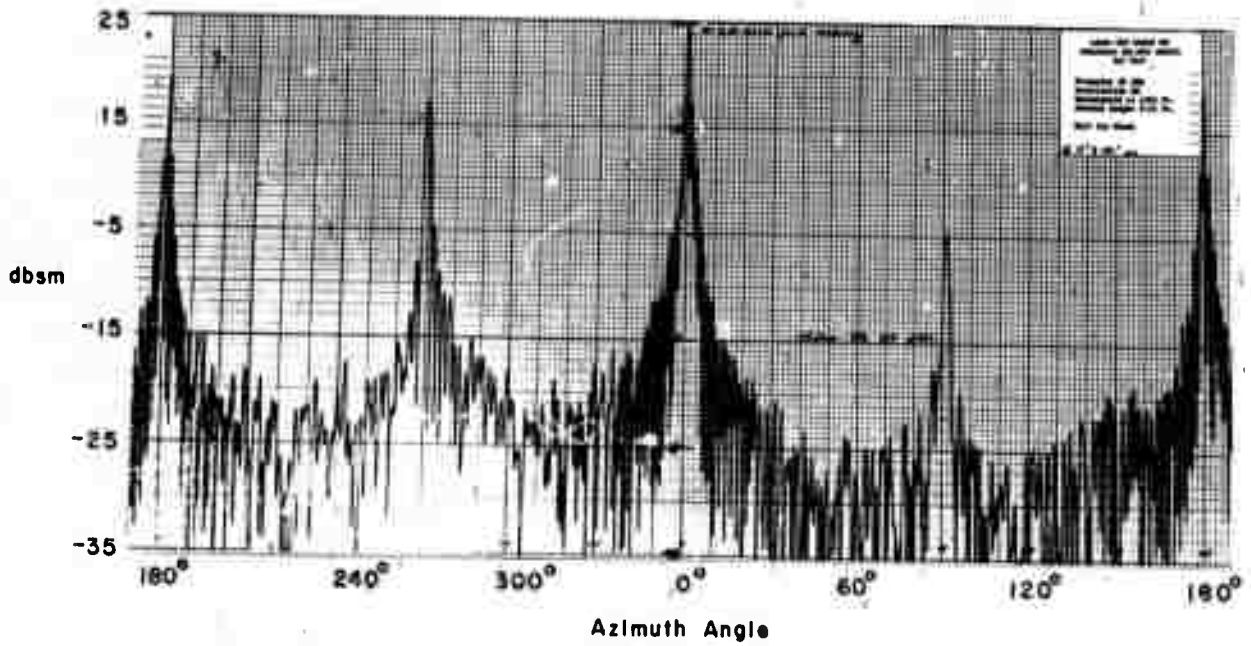

d. Block of salt-water ice.

Figure 31 (Cont'd).

Table XI. Reflection coefficients for normal incidence on a 10 × 10 × 5-in. face of ice block placed on rotator at horizontal polarization at 10 and 35 GHz.

Object	Face dimensions (in.)	Azimuth (°)	Frequency (GHz)	Calculated (dbsm)	Measured (dbsm)	Reflection coefficient (R)
Pure ice	10 × 10	0	10	17.7	6.5	0.076
	10 × 10	180	10	17.7	−6.0	0.0054
	10 × 5	90	10	14.7	4.0	0.084
	10 × 5	270	10	14.7	1.5	0.0047
Salt ice	10 × 10	0	10	17.7	7.0	0.0187
	10 × 10	180	10	17.7	−4.0	0.0174
	10 × 5	90	10	14.7	−1.0	0.0270
	10 × 5	270	10	14.7	1.0	0.0355
Pure ice	10 × 10	0	35	28.5	9.0	0.011
	10 × 10	180	35	28.5	13.5	0.031
	10 × 5	90	35	24.3	3.5	0.008
	10 × 5	270	35	24.3	4.0	0.009
Salt ice	10 × 10	0	35	28.5	15.0	0.045
	10 × 10	180	35	28.5	9.5	0.013
	10 × 5	90	35	24.3	−5.0	0.001
	10 × 5	270	35	24.3	7.5	0.020

Table XI gives the values of R for horizontal polarization at azimuth angles of 0°, 90°, 180° and 270°. The reflection coefficients show large variations among the different blocks. Theoretically, the power reflection coefficient for ice with a relative dielectric constant of 3 is 0.13. In all test cases, the measured power reflection coefficient was less than 0.13, indicating destructive interference between reflections from front and back surfaces and perhaps internal reflections.

Because the reflection is dependent on both the dielectric constant and the thickness of the block, the difference between returns from salt ice blocks and those from fresh-water ice blocks is not distinguishable. Perhaps the main distinction between the returns from salt ice and those from fresh-water ice can be observed in the lobing patterns (e.g., Fig. 31c and d).

The radar cross sections of ice blocks placed on a rotator in free space are about 10 dbsm higher than those of the ice blocks placed on the snow surface. The difference is probably caused by the ground lobing structure and the greater roughness of the ice blocks placed on the snow surface.

LITERATURE CITED

Battles, J.W. and D.E. Crane (1966) Attenuation of *Ka*-band energy by snow and ice. U.S. Naval Ordnance Laboratory, Corona, California, 10 Aug (AD 638303).

Cummings, W.A. (1952) The dielectric properties of ice and snow at 3.2 cm. *Journal of Applied Physics*, vol. 23, no. 7, p. 768.

Eisenberg, D. and W. Kauzmann (1969) *Structure and properties of water.* New York: Oxford University Press.

Hoekstra, P. and P. Cappillino (1971) The dielectric properties of sea ice at UHF and microwave frequencies. *Journal of Geophysical Research*, vol. 76, p. 4922.

LITERATURE CITED (Cont'd)

Lamb, J. and A. Turney (1949) The dielectric properties of ice at 1.25-cm wavelength. *Proceedings of the Physical Society*, Sec. B, vol. 62, pt. 4, p. 272.

Lofgren, G. and W.F. Weeks (1969) Effect of growth parameters on substructure spacing in NaCl ice. *Journal of Geophysical Research*, vol. 73, p. 153.

Saxton, J.A. (1950) Reflection coefficient of snow and ice at V.H.F. *Wireless Engineer*, vol. 27, p. 17.

Suzuki, M. and T. Hasegawa (1958) Studies on the reflection of microwaves on a snow-covered terrain. In *Microwave propagation in snowy districts* (Y. Asami, Ed.), Research Institute of Applied Electricity, Hokkaido University, Sapporo, Japan.

Waite, A.H., Jr. (1965) The international cooperative experiment on glacial sounding. Sponsored by U.S. Army Electronics Command (USAEC) and U.S. Army Cold Regions Research and Engineering Laboratory (USA CRREL), Greenland, 1963 and 1964. USAEC Internal Report, 15 Sept (unpublished).